J. Fluid Mech. (1998), *vol.* 365, *pp.* 269–303. Printed in the United Kingdom

On stability of streamwise streaks and transition thresholds in plane channel flows

By SATISH C. REDDY[1], PETER J. SCHMID[2], JEFFREY S. BAGGETT[3] AND DAN S. HENNINGSON[4]†

[1]Department of Mathematics, Oregon State University, Corvallis, OR 97331, USA
e-mail: reddy@math.orst.edu

[2]Department of Applied Mathematics, University of Washington, Box 352420, Seattle, WA 98195-2420, USA
e-mail: pjs@amath.washington.edu

[3]Center for Turbulence Research, Building 500, Stanford University, Stanford, CA 94305-3030, USA
e-mail: baggett@ctr-sgi1.stanford.edu

[4]The Aeronautical Research Institute of Sweden (FFA), Box 11021, S-161 11 Bromma, Sweden
e-mail: hnd@ffa.se

(Received 15 April 1996 and in revised form 29 January 1998)

Streak breakdown caused by a spanwise inflectional instability is one phase of the following transition scenarios, which occur in plane Poiseuille and Couette flow. The streamwise vortex scenario is described by

(SV) streamwise vortices $\Longrightarrow$ streamwise streaks $\Longrightarrow$
streak breakdown $\Longrightarrow$ transition.

The oblique wave scenario is described by

(OW) oblique waves $\Longrightarrow$ streamwise vortices $\Longrightarrow$ streamwise streaks $\Longrightarrow$
streak breakdown $\Longrightarrow$ transition.

The purpose of this paper is to investigate the streak breakdown phase of the above scenarios by a linear stability analysis and compare threshold energies for transition for the above scenarios with those for transition initiated by Tollmien–Schlichting waves (TS), two-dimensional optimals (2DOPT), and random noise (N) at subcritical Reynolds numbers.

We find that if instability occurs, it is confined to disturbances with streamwise wavenumbers α_0 satisfying $0 < \alpha_{min} < |\alpha_0| < \alpha_{max}$. In these unstable cases, the least stable mode is located near the centre of the channel with a phase velocity approximately equal to the centreline velocity of the mean flow. Growth rates for instability increase with streak amplitude. For Couette flow streak breakdown is inhibited by mean shear. Using the linear stability analysis, we determine lower bounds on threshold amplitude for transition for scenario (SV) that are consistent with thresholds determined by direct numerical simulations.

In the final part of the paper we show that the threshold energies for transition in Poiseuille flow at subcritical Reynolds numbers for scenarios (SV) and (OW) are two orders of magnitude lower than the threshold for transition initiated by Tollmien–Schlichting waves (TS) and an order of magnitude lower than that for

† Also at Department of Mechanics, Royal Institute of Technology (KTH), S-100 44 Stockholm, Sweden

(2DOPT). Scenarios (SV) and (OW) occur on a viscous time scale. However, even when transition times are taken into account, the threshold energy required for transition at a given time for (SV) and (OW) is lower than that for the (TS) and (2DOPT) scenarios at Reynolds number 1500.

1. Introduction

Despite more than a century of research and much progress, transition to turbulence is still not completely understood – even in relatively simple flows such as plane Poiseuille and Couette flow.

In the non-dimensionalized geometry channel flow is between infinite horizontal plates at $y = -1$ and $y = 1$. All distances are non-dimensionalized by the half-channel height, h, and all velocities by the difference between the wall and centreline velocities, V_d. We define the Reynolds number as $R = hV_d/\nu$, where ν is the kinematic viscosity. Poiseuille and Couette flow have non-dimensionalized velocity profiles $U = 1 - y^2$ and $U = y$, respectively.

Traditionally, a first step in investigating transition is linear stability analysis. The Navier–Stokes equations are linearized about the laminar flow and solutions growing exponentially in time are sought (Drazin & Reid 1981). Linear stability analysis predicts that plane Poiseuille flow is stable for $R < 5772$ (Orszag 1971) and plane Couette flow is stable for all Reynolds numbers (Romanov 1973).

However, transition experiments show that plane Poiseuille flow undergoes transition to turbulence for R as low as 1000 (Patel & Head 1969) and for plane Couette flow the transitional Reynolds number is in the range $325 \leqslant R \leqslant 370$ (Lundbladh & Johansson 1992; Tillmark & Alfredsson 1992; Dauchot & Daviaud 1995*a*). The precise path to transition depends on a number of factors, including the background noise environment (Morkovin & Reshotko 1990; Reshotko 1994). The discrepancies between experiments and linear stability analysis have led to much research on nonlinear theories.

One such theory is the secondary instability theory of Tollmien–Schlichting (TS) waves (see for example Klebanoff, Tidstrom & Sargent 1962; Orszag & Patera 1983; Bayly, Orszag & Herbert 1988; Herbert 1988). This transition scenario is shown schematically as

(TS) 2D TS wave $\Longrightarrow$ 2D state $\Longrightarrow$ 2D state breakdown $\Longrightarrow$ transition.

The usual initial condition is a finite-amplitude TS wave, the eigenfunction of the Orr–Sommerfeld equation with the greatest growth rate. The finite-amplitude TS wave evolves nonlinearly into a two-dimensional equilibrium state in Poiseuille flow if $R > 2900$. For $R < 2900$ in Poiseuille flow and all Reynolds numbers in Couette flow the two-dimensional state decays. The two-dimensional state is linearly unstable to three-dimensional disturbances. This secondary instability is active at Reynolds numbers as low as ≈ 1000 in Poiseuille and Couette flows.

While this transition scenario agrees qualitatively and quantitatively with experiments where a two-dimensional TS wave is introduced in the flow via a vibrating ribbon (see the reviews by Bayly *et al.* (1988) and Herbert (1988)), it does not seem to completely describe natural transition in plane channel flows. First, natural transition is three-dimensional from the outset (Klingmann 1992). Secondly, as we show here, at subcritical Reynolds numbers the energy of the TS wave required to initiate

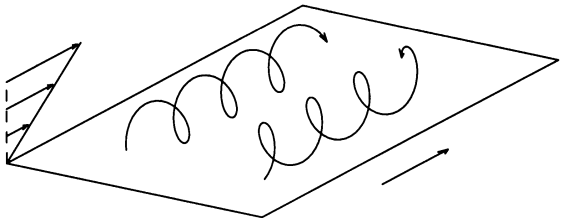

FIGURE 1. Counter-rotating streamwise vortices in Couette flow taken from Trefethen *et al.* (1993).

transition is greater than the energy of other three-dimensional disturbances which lead to transition. Finally, the TS waves are no longer secondarily unstable for R less than approximately 1000 in plane Couette flow, whereas transition can occur at much lower Reynolds numbers.

Recently, there has been an intense re-examination of the linearized Navier–Stokes equations. Linear stability implies that the disturbance energy of sufficiently small perturbations to the laminar flow decays to 0 as $t \to \infty$. But for finite times the energy of disturbances may grow linearly by as much as $O(R^2)$ before decaying (Boberg & Brosa 1988; Kim & Moser 1989; Gustavsson 1991; Butler & Farrell 1992; Reddy & Henningson 1993). For a given streamwise and spanwise wavenumber one can determine a disturbance, called an optimal, which yields the greatest transient linear growth. In channel flows, the optimals which yield the most disturbance growth are independent, or nearly independent, of the streamwise coordinate. Physically, transient growth results from the redistribution of streamwise momentum by small velocity perturbations in the direction normal to the shear. Mathematically, transient growth can be explained by the fact that the linearized Navier–Stokes operator has non-orthogonal eigenfunctions. An overview of recent work can be found in review articles (Trefethen *et al.* 1993; Henningson 1995). Experiments and numerical simulations indicate that transient growth mechanisms play a fundamental role in the initial stages of transition in channel and pipe flows (Klingmann 1992; Schmid & Henningson 1992; Henningson, Lundbladh & Johansson 1993; Mayer & Reshotko 1997).

In this paper, we present two scenarios in which transition is initiated by optimal disturbances in plane Poiseuille and plane Couette flow. As in the (TS) scenario, a secondary instability occurs. An array of streamwise streaks periodic in the spanwise direction is the unstable flow configuration.

First, we consider transition initiated by streamwise vortices – the optimals with no streamwise dependence. We focus on streamwise vortices because they yield the most transient linear growth and because they are ubiquitous features in many shear flows. Schematically, the (SV) scenario is

(SV) streamwise vortices $\Longrightarrow$ streamwise streaks $\Longrightarrow$
streak breakdown $\Longrightarrow$ transition.

This route to turbulence occurs in a number of flow geometries including flow above a concave wall and curved channel flow; we discuss these further in § 2. These flows are linearly unstable and the least-stable mode is in the form of streamwise vortices. The streamwise vortices are no longer unstable eigenmodes in plane channel flows, but they have the greatest potential for transient growth, suggesting that transition may be initiated by relatively low-energy disturbances.

We present an example of scenario (SV) in Couette flow. Figure 1 shows the initial

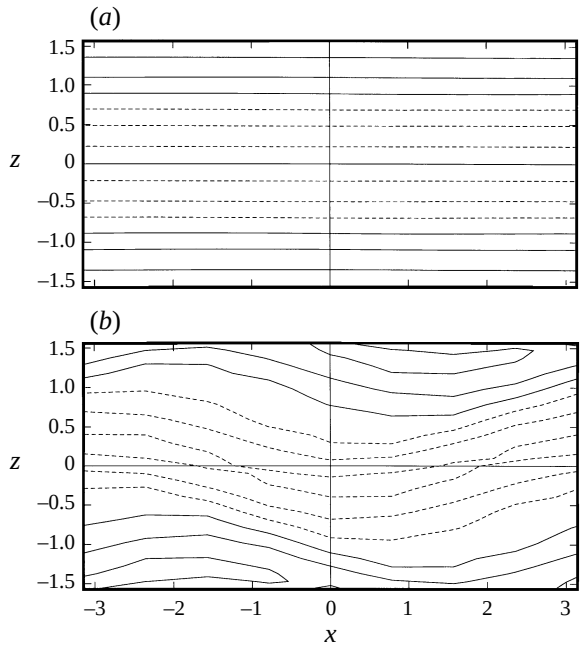

FIGURE 2. Streaks and their breakdown in Couette flow. The flow is in the x-direction. The plots show contours of the streamwise velocity in the plane $y = 0$. The contours start at -0.5 and have spacing 0.2. (*a*) The field at $t = 30$, consisting of flow moving to the left (dashed contours) and right (solid contours). (*b*) At $t = 60$ the flow is undergoing an instability. In this simulation transition occurs at $t \approx 67$.

disturbance, an array of counter-rotating vortices periodic in the spanwise z-direction plus streamwise-dependent noise of $\approx 1\%$ of the vortex energy. We emphasize that transition cannot take place in the absence of streamwise-dependent structures. Let x denote the streamwise direction and y the wall-normal direction. The vortices create streamwise streaks of high- and low-speed fluid by the lift-up mechanism (Landahl 1975), as shown in figure 2. High (low)-speed fluid is advected downwards (upwards) by the vortices as shown in figure 2(*a*). If the streak amplitude is sufficiently large, the streaks break down, as shown in figure 2(*b*). In this simulation transition occurs at $t \approx 67$. However, streak breakdown need not yield transition.

The streak breakdown is similar to a Kelvin–Helmholtz instability. As the vortices evolve, the streamwise velocity profile $U(y, z)$ of the streaks develops inflection points in both the normal y- and spanwise z-directions; see figure 3. The main conclusion of recent work is that the streak breakdown is primarily a spanwise inflectional instability.

The second route to turbulence we consider begins with a pair of optimal oblique waves. The oblique waves are chosen so that they each grow linearly via the transient growth mechanism. The pair of growing waves interact nonlinearly to create streamwise-independent structures including streamwise vortices. Schematically, the oblique wave (OW) scenario is

(OW) oblique waves $\Longrightarrow$ streamwise vortices $\Longrightarrow$ streamwise streaks $\Longrightarrow$ streak breakdown $\Longrightarrow$ transition.

Except for the first stage, this route to turbulence is similar to (SV). This scenario has been investigated in Poiseuille flow (Schmid & Henningson 1992; Schmid, Lundbladh

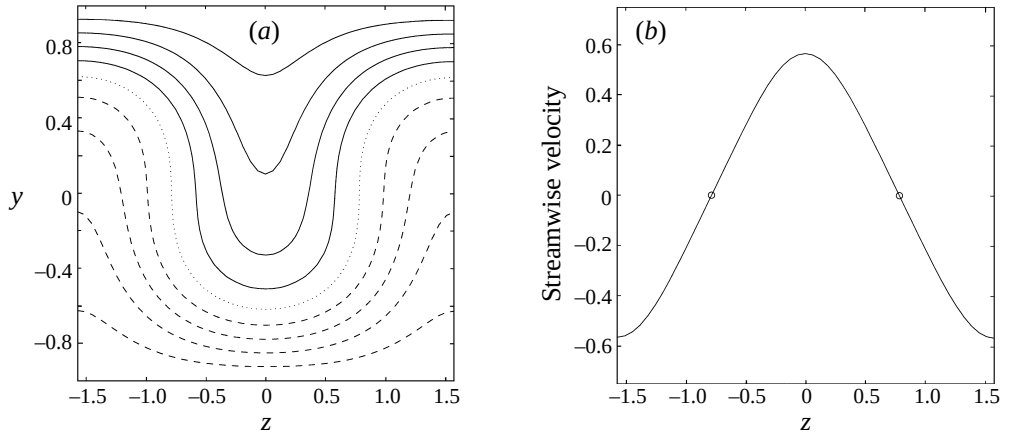

FIGURE 3. Plot (*a*) Contours of the streamwise velocity $U(y, z)$ at $t = 30$ in the simulation described in figure 2 in the absence of noise. The contour values from bottom to top are $-0.8, -0.6, -0.4, \ldots, 0.8$; negative contours are dashed, positive are solid, and the zero contour is dotted. (*b*) The spanwise streak velocity profile at the centreline, $U(0, z)$. The circles are the inflection points.

& Henningson 1994; Elofsson & Alfredsson 1994) and in various other flow geometries, including incompressible boundary layers (Joslin, Streett & Chang 1993; Berlin, Lundbladh & Henningson 1994), compressible boundary layers (Fasel & Thumm 1991; Chang & Malik 1994), and compressible shear layers (Gathmann, Si-Ameur & Mathey 1993).

Transition to turbulence at subcritical Reynolds numbers requires a finite-amplitude disturbance to the laminar solution. The threshold energy is defined to be the minimum initial disturbance energy for transition. Comparing the threshold energies gives a measure of the likelihood that a particular scenario occurs in a slightly disturbed flow. In previous work the threshold for transition for scenarios (SV) and (OW) in Poiseuille and Couette flow was approximated by direct numerical simulations (Kreiss, Lundbladh & Henningson 1994; Lundbladh, Henningson & Reddy 1994). For (SV), the threshold energy scales like R^{-2} for $500 \leqslant R \leqslant 4000$ in Couette flow and $R^{-7/2}$ for $1500 \leqslant R \leqslant 5000$ in Poiseuille flow. For scenario (OW) the thresholds are approximately $R^{-5/2}$ and $R^{-7/2}$ for Couette and Poiseuille flow, respectively. Although the potential for linear transient growth is lower for oblique waves than for streamwise vortices, the threshold is lower for (OW) than for (SV).

The question of thresholds for transition initiated by streamwise vortices was considered previously by Hamilton & Abernathy (1994), who did experiments in water table flow. They found that strong vortices ultimately led to transition, whereas weak vortices did not, but they were unable to determine a precise value of the vortex strength for transition. They conclude that the existence of inflection points in the spanwise velocity profile is necessary but not sufficient for transition to occur.

The purpose of this paper is threefold.

(i) Investigate the streak breakdown phase of the streamwise vortex and oblique wave scenarios. In particular, we are interested in the relationship between the threshold for streak breakdown and the threshold for transition in scenario (SV).

(ii) Understand why smaller streamwise vortices lead to transition in plane Poiseuille flow than in plane Couette flow, even though the transient growth of streamwise vortices is quantitatively similar in both flows.

(iii) Show that the thresholds for transition for the streamwise vortex and oblique wave scenarios are substantially lower than the threshold for transition from Tollmien–Schlichting waves.

Streak breakdown in the spatial setting at subcritical Reynolds numbers in Poiseuille flow has recently been investigated experimentally by Kawakami, Elofsson & Alfredsson (1997). Streak breakdown has also been considered in turbulent channel flows. Hamilton, Kim & Waleffe (1995) and Waleffe (1995*a*) studied streak breakdown in Couette flow via direct numerical simulations and linear stability analysis. Coughlin (1996) investigated streak breakdown in both Couette and Poiseuille flows via direct numerical simulations. In these papers, streak breakdown is one phase of a self-sustaining cycle which forms the backbone of the turbulent state. Our direct simulations and linear stability analysis are similar to those in Hamilton *et al.* (1995) and Coughlin (1996). The present paper extends this previous work in several directions as outlined below.

Section 2 gives further details on the breakdown of streamwise streaks as it occurs in a number of flow geometries. Section 3 describes the simulation code and § 4 presents results on growth rates for streak breakdown from direct numerical simulations.

Section 5 presents results on growth rates from a linear stability analysis for both Couette and Poiseuille flow. We find good agreement between simulations and linear analysis. An analysis of the dependence of the growth rate on the initial vortex amplitude is presented. We find that shear in the wall-normal direction at the centre of the channel provided by the underlying base flow can inhibit the breakdown of streaks; a model problem is presented and analysed to demonstrate this. This phenomenon differentiates Poiseuille flow, where the shear at the centre is 0, from Couette flow, where the shear is non-zero. We end this section by showing that the growth rates for the fundamental-type instability are greater than those for the subharmonic-type instability.

Section 6 presents a brief discussion of the oblique wave transition scenario. Section 7 compares the thresholds for streak breakdown with the threshold for transition from streamwise vortices. As expected, the streak instability is necessary but not sufficient for transition. We also examine the differences in the threshold scalings for the two flows.

Section 8 compares the threshold energy for transition in (SV) and (OW) with that of (TS). The threshold energy for the secondary instability scenario is about 2 orders of magnitude smaller in (SV) and (OW) than in (TS); see figure 19. If a two-dimensional optimal disturbance (2DOPT) is used as an initial condition in the secondary instability scenario, the discrepancy is only an order of magnitude. Furthermore, even though transition in (SV) and (OW) takes place on a time scale $O(R)$ (the time for development of the streaks) as compared to the $O(1)$ time scale for (TS), we show that the threshold energy for (OW) is still two orders of magnitude smaller than that for (TS) and an order of magnitude lower than that for (2DOPT) over comparable times scales at $R = 1500$. The threshold for (SV) is an order of magnitude lower than that for (TS) and a factor 3 lower than that for two-dimensional optimals; see figure 21.

2. Streak breakdown

Transition initiated by streamwise vortices as in scenario (SV) occurs in a number of flow geometries, including flow over a curved wall and in curved channel flow. These flows are linearly unstable, with streamwise vortices as the primary instability.

In channel flow, streamwise vortices are not a primary linear instability. This is probably the reason why scenario (SV) has received little attention in channel flow.

In flow over a curved wall the vortices are called Görtler vortices; see Saric (1994) for a review. In this geometry there are two types of unstable modes. In most cases, the most unstable is a sinuous mode, similar to that in figure 2. In addition, there is a varicose mode, which is symmetric in the spanwise direction. Streak breakdown was studied experimentally by Swearingen and Blackwelder (1987). The breakdown was studied by an inviscid linear analysis by Hall & Horseman (1991). By an energy analysis, Yu & Liu (1994) showed that the sinuous and varicose modes are correlated with inflection points in the spanwise and streamwise directions, respectively. Li & Malik (1995) performed an inviscid linear stability analysis and found that for some parameter combinations the varicose mode is the most unstable.

In curved channel flow driven by a pressure gradient, Dean vortices develop if the Reynolds number is sufficiently large. By linear analysis and direct simulations, Finlay, Keller & Ferziger (1988) found two types of instability. Spanwise inflection instability occurs for Reynolds numbers R above twice the critical value R_c for the primary instability. In addition there is a second instability, called undulating, that occurs if $R > 1.3R_c$. By considering one-dimensional streak profiles of the form $U(y)$ and $U(z)$, Le Cunff & Bottaro (1993) concluded that the undulating instability is centrifugal in nature. Matsson & Alfredsson (1992) observed the spanwise inflectional instability experimentally.

Streak breakdown also occurs in flows above a flat plate. Fischer & Dallmann (1991) investigated the primary and secondary instability of a three-dimensional boundary layer using a laminar Falkner–Skan–Cook profile and a spanwise-varying finite-amplitude state obtained from measurements. They found good agreement between a secondary instability analysis and experimental results. Bakchinov *et al.* (1995) observe streak breakdown experimentally by directly putting streamwise vortices in the flow. Matsubara & Alfredsson (1995) observe instability, as in figure 2, just before breakdown of streaks into turbulent spots.

Kawakami *et al.* (1997) recently performed experiments on streak breakdown in the spatial setting in plane Poiseuille flow at Reynolds numbers in the range 2000–2900. They created streaky structure with suction and found that the least-stable mode is sinuous and that breakdown occurs only if the streak amplitude exceeds a certain threshold. They found that growth rates are independent of the Reynolds number in the above range. Comparisons with results in the present paper are given below.

Streaky structures elongated in the streamwise direction play a fundamental role in the sustainment of turbulence in wall-bounded shear flows (Kline *et al.* 1967; Kim, Kline & Reynolds 1971), and much work has been done on the origin and breakdown of these structures in the turbulent regime. An analysis of streak breakdown in channel flow is presented in recent papers on near-wall turbulence by Hamilton *et al.* (1995), Waleffe (1995*a*) and Coughlin (1996). In the model considered in these papers, streak breakdown is one phase of a self-sustaining cycle in turbulent flow, which includes streak formation, streak breakdown, and streamwise vortex regeneration from the direct nonlinear interaction of the streak instability eigenmode.

Dauchot & Daviaud (1995*b*) investigated the evolution of streamwise vortices in Couette flow by placing a wire in the flow. They found that if the Reynolds number is above 160, streamwise vortices are continuously shed from the wire and create streaks. The streaks and vortices extend a finite distance from the wire, with the distance increasing with Reynolds number. Above $R = 340$, the vortices break down

and turbulence appears. Evidence of a streak breakdown as in the Introduction is not apparent.

Finally, we note that Zikanov (1996) has recently investigated scenario (SV) in incompressible pipe flow by direct simulations. The scenario appears to be the same as in the other flow geometries.

3. Description of numerical techniques

The simulations in this paper are done using a program that solves the full three-dimensional Navier–Stokes equations in the channel flow geometry (Lundbladh *et al.* 1992). The program uses Fourier series in the streamwise (x) and spanwise (z) directions and Chebyshev series in the normal (y) direction. Time integration is done by a fourth-order Runge–Kutta formula for the nonlinear terms and a second-order Crank–Nicholson method for the linear terms. Aliasing errors are removed by the $\frac{3}{2}$-rule when the FFTs are calculated. For Poiseuille flow constant mass flux is assumed. The code has been tested thoroughly and has been run on various workstations and supercomputers.

The flow is assumed to be periodic in the homogeneous directions with lengths L_x and L_z in the streamwise and spanwise directions, respectively. The fundamental wavenumbers are $\alpha_f = 2\pi/L_x$ and $\beta_f = 2\pi/L_z$. The length in the wall-normal direction is fixed at 2.

Our results on thresholds are expressed in terms of energy density of initial disturbances. The energy density of a disturbance is given by

$$E = \frac{1}{2V}\int_{period}(u^2 + v^2 + w^2)\mathrm{d}\boldsymbol{x}, \tag{1}$$

where u, v, w are the perturbation velocities, the region of integration is one periodic box, and V is the volume of the periodic box. We can re-write (1) for the case of a wave-like disturbance of the form

$$\mathrm{Re}\{(\bar{u}(y), \bar{v}(y), \bar{w}(y))\mathrm{e}^{\mathrm{i}\alpha x + \mathrm{i}\beta z}\},$$

where α and β are the streamwise and spanwise wavenumbers. Defining the normal vorticity function as $\bar{\eta} = \mathrm{i}\beta\bar{u} - \mathrm{i}\alpha\bar{w}$ and $k^2 = \alpha^2 + \beta^2$, we have

$$E = \frac{1}{8k^2}\int_{-1}^{1}\left(\left|\frac{\mathrm{d}\bar{v}}{\mathrm{d}y}\right|^2 + k^2|\bar{v}|^2 + |\bar{\eta}|^2\right)\mathrm{d}y.$$

In our computations of transition for the three scenarios random noise with total energy density 1% of the primary disturbance energy density is added to modes with streamwise wavenumber $0, \pm\alpha_f, \pm 2\alpha_f$ and spanwise wavenumber $0, \pm\beta_f, \pm 2\beta_f$. The noise is in the form of Stokes modes. Noise is necessary for transition for scenarios (SV) and (TS), but is not required for scenario (OW).

The initial disturbances in simulations of scenario (TS) are determined by solving the Orr–Sommerfeld equation for the least-stable mode. For scenarios (SV), (OW), and (2DOPT) the initial disturbances are optimal streamwise vortices, oblique waves, and two-dimensional waves, respectively. The optimals have the greatest potential for transient growth in the linear case. The computations of initial disturbances are done by spectral methods (Reddy & Henningson 1993).

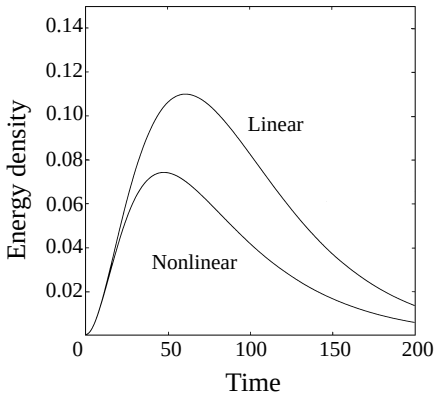

FIGURE 4. Disturbance energy for linear and nonlinear evolution of a finite-amplitude initial optimal streamwise vortex in Couette flow. (See Case 2 below.)

4. Direct numerical simulations of streak breakdown

We begin with an examination of the streak breakdown phase of the streamwise vortex scenario by direct simulations. The initial streamwise vortex has the form

$$\mathrm{Re}\{(U_1(y,t=0),V_1(y,t=0),W_1(y,t=0))\mathrm{e}^{\mathrm{i}\beta_0 z}\}. \tag{2}$$

The vector function $\boldsymbol{U}_1(y,t=0)$ is chosen so it is an optimal. Roughly speaking, the optimal disturbance is configured so that most of the energy is in the normal velocity component.

As the initial streamwise vortex evolves it generates streamwise velocity. For the inviscid linear case, Ellingsen & Palm (1975) showed that $V_1(y,t)$ is constant and that the streamwise disturbance velocity has the form

$$U_1(y,t) = U_1(y,0) - U'(y)V_1(y,t)t, \tag{3}$$

where $U(y)$ is the laminar velocity profile. Landahl (1980) extended this result to the linear evolution of localized disturbances.

Viscosity shuts off the growth of streamwise disturbances. In the linear evolution of an optimal vortex in viscous flow the maximum energy growth occurs at a time $O(R)$ as $R \to \infty$ (Kim & Moser 1989; Gustavsson 1991; Butler & Farrell 1992; Reddy & Henningson 1993). At this time, the streamwise disturbance velocity is roughly $O(\epsilon R)$, where ϵ is the amplitude of the initial normal velocity. This corresponds to energy growth by a factor $O(R^2)$.

Figure 4 shows the disturbance energy of an evolving optimal vortex in Couette flow at $R = 500$ in the absence of noise for $\beta_0 = 2$. In Poiseuille flow the greatest linear transient growth occurs close to this wavenumber. In Couette flow the greatest transient growth occurs for $\beta_0 \approx 1.66$. The initial energy density is 4×10^{-4}. If the disturbance is evolved linearly, there is energy growth by a factor ≈ 275. In the full nonlinear simulation energy is extracted from the mean flow as the streaks grow and the shear which drives the streaks is reduced so that the streaks do not grow to their full linear potential. In the nonlinear evolution, higher harmonics with spanwise wavenumbers $k\beta_0$ for $k = 2,3,\ldots$, are generated and the mean flow, which is initially the linear profile $\boldsymbol{U} = (y,0,0)$, is modified.

For this simulation and the rest in this section the periodic box has dimensions $8\pi \times 2 \times \pi$. We use 49 discretization points in the y-direction and 32 Fourier modes in the x- and z-directions.

Case	Flow	R	β_0	Ampl.	E_v	E_s
1	Couette	500	2	1.0×10^{-2}	2.5×10^{-5}	4.2×10^{-3}
2	Couette	500	2	4.0×10^{-2}	4.0×10^{-4}	6.2×10^{-2}
3	Poiseuille	1500	2	2.0×10^{-2}	1.0×10^{-4}	1.5×10^{-2}

TABLE 1. Summary of simulation parameters. The fifth column gives the amplitude of the initial vortex. The final two columns give the energy density of the initial vortex, E_v, and the streak, E_s.

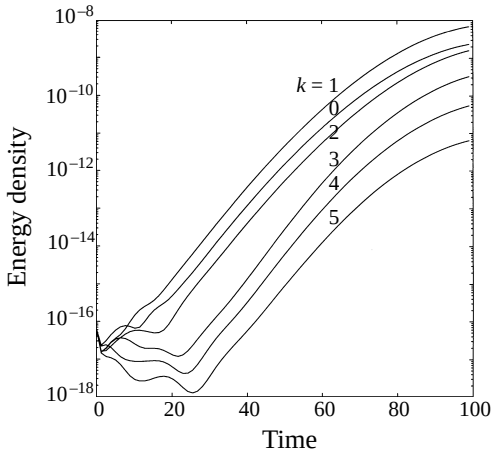

FIGURE 5. Energy density in the wavenumbers $(\alpha_0, k\beta_0)$, for $k = 0, 1, 2, 3, 4, 5$ for Couette flow with $R = 500$ (Case 2). Here $\alpha_0 = 0.75$ and $\beta_0 = 2$.

Note that the disturbance eventually dies out in both the linear and nonlinear simulations. In the linear case the decay is exponential with decay rate $O(1/R)$. Hence, the streak profile, as shown in figure 2, is not steady. In the stability calculations of the next sections we make the assumption that the time scale for decay of streaks is slower than that for streak breakdown.

Our goal is to investigate the stability of streaks generated by the initial optimal vortices. We consider three cases, summarized in table 1. For the Couette flow cases, we take the velocity field that evolves from the initial streamwise vortices after 30 time units. For the Poiseuille flow case, we take the field at $t = 40$. The initial amplitude is defined as $A = 2E_v^{1/2}$. We add a small perturbation of the form

$$\boldsymbol{U}_{\text{pert}} = \text{Re}\left\{ e^{i\alpha_0 x} \sum_{k=-15}^{15} \boldsymbol{F}_k(y) e^{ik\beta_0 z} \right\}$$

to the streak field. The energy density of the perturbation is $\approx 10^{-15}$. Here α_0 is the streamwise wavenumber of the perturbation. The functions $\{\boldsymbol{F}_k\}$ are random linear combinations of Stokes modes (Lundbladh, Henningson & Johansson 1992). The evolution of the disturbance consisting of the streak and the perturbation is computed by the simulation code.

Figure 5 plots the energy density of the perturbation in various modes for $\alpha_0 = 0.75$ for Case 2. After an initial transient phase, the energy density grows or decays exponentially; see also (Hamilton *et al.* 1995). If we assume that the energy density in a particular wavenumber behaves like $Ce^{2\gamma(t-t_0)}$ for the straight part of the curve, then

we define γ to be the growth rate. For the case considered in figure 5 we find that the growth rate is approximately 0.14. We have done similar calculations for other values of the streamwise wavenumber α_0 and also for Cases 1 and 3.

The approach taken here is similar to that in (Hamilton, Kim & Waleffe 1995), where the streak profile is taken from a simulation of turbulent flow. However, in their work the streak profile is 'frozen'. They report some differences between simulations in which the streaks are artificially frozen and those in which the streaks are allowed to evolve. Coughlin (1996) also performed similar computations, but used a small amount of forcing to maintain the streamwise vortices and streaks in a steady equilibrium. For Poiseuille flow and low levels of forcing in Couette flow a constant growth rate is found. For high levels of forcing in Couette flow, the growth rate varies periodically with time. We have not investigated this phenomenon.

5. Linear stability analysis

We model the above results by a linear stability analysis. There are several standard assumptions that greatly simplify the linear stability equations (Hall & Horseman 1991; Yu & Liu 1994; Li & Malik 1995; Finlay *et al.* 1988; Waleffe 1995*a*).

(*a*) The normal and spanwise components of the velocity field for the streak are negligible. This is verified in the numerical simulations of the previous section. For example, for the high-amplitude streaks in Couette flow the streamwise component contributes more than 99% of the disturbance energy.†

(*b*) The streak profile does not depend on the streamwise coordinate x. If the initial vortex does not depend on x, then the streak profile does not depend on x.

(*c*) We assume that the time scale for decay of streaks is longer than the time scale for streak instability. As figure 4 shows, streaks eventually decay in the absence of noise. In our computations we take the streak profile to be time-independent.

We assume a streak velocity field of the form $\boldsymbol{U} = (U(y,z,t),0,0)$. The velocity field is periodic in the spanwise direction and can be expressed in the form

$$U(y,z,t) = \mathrm{Re}\left\{ U_0(y,t) + 2\sum_{k=1}^{\infty} U_k(y,t)\mathrm{e}^{\mathrm{i}\beta_0 kz} \right\}. \tag{4}$$

For the simulations of the previous section, the functions $\{U_k\}$ decay to zero rapidly as $k \to \infty$. As mentioned in (*c*), we take the streak profile at fixed t and assume that it is steady in the linear stability calculations.

To study the stability of the streak we substitute $\boldsymbol{U} + \boldsymbol{u}$, where $\boldsymbol{u}(x,y,z,t) = (u,v,w)$ is the perturbation velocity, into the Navier–Stokes equations. The resulting linear equations and the solution technique are similar to those in Waleffe (1995*a*). For completeness we have included the equations in Appendix A.

We assume that the perturbation normal velocity and normal vorticity have the form

$$v(x,y,z,t) = \mathrm{Re}\left\{ \mathrm{e}^{\mathrm{i}\alpha_0 x - \mathrm{i}ct} \sum_{k=-m}^{m} v_k(y)\mathrm{e}^{\mathrm{i}k\beta_0 z} \right\}, \tag{5}$$

$$\eta(x,y,z,t) = \mathrm{Re}\left\{ \mathrm{e}^{\mathrm{i}\alpha_0 x - \mathrm{i}ct} \sum_{k=-m}^{m} \eta_k(y)\mathrm{e}^{\mathrm{i}k\beta_0 z} \right\}, \tag{6}$$

† It was pointed out in a private communication (Waleffe 1994), that it is not only the size of the velocity components themselves but their gradients which is of importance in the stability analysis.

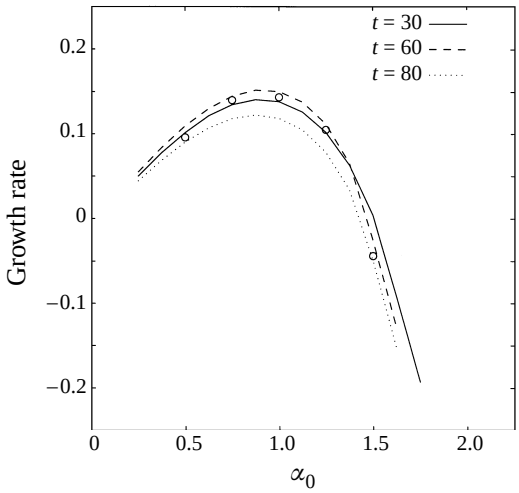

FIGURE 6. Comparison of growth rate results from direct numerical simulations and linear stability analysis for high-amplitude streaks in Couette flow with $R = 500$. The small circles are the results obtained from the direct numerical simulations of § 4.

where α_0 and β_0 are the fundamental streamwise and spanwise wavenumbers, respectively. To simplify the stability calculations further we assume that the quantities $\{U_i(y,t)\}$ all have phase 0. (This is the case in the examples of the previous section.) In this case, sinuous and varicose modes can be considered separately. The term sinuous refers to disturbances for which v and η are odd and even functions of z, respectively:

$$v(x,y,z,t) = \mathrm{Re}\left\{2\mathrm{i}e^{\mathrm{i}\alpha_0 x - \mathrm{i}ct}\sum_{k=1}^{m} v_k(y)\sin(k\beta_0 z)\right\}, \tag{7}$$

$$\eta(x,y,z,t) = \mathrm{Re}\left\{e^{\mathrm{i}\alpha_0 x - \mathrm{i}ct}\left(\eta_0(y) + 2\sum_{k=1}^{m}\eta_k(y)\cos(k\beta_0 z)\right)\right\}. \tag{8}$$

To derive the stability equations we substitute (7) and (8) into (A 5) and (A 6) and collect terms with like powers of $e^{i\beta_0 z}$. This yields a differential eigenvalue problem for the unknown eigenvalue c and the corresponding vorticity and velocity components, $\{\eta_k\}$ and $\{v_k\}$. We have developed a code based on a Chebyshev collocation discretization for solving this eigenvalue problem. The code takes as input the terms $\{U_i\}$ in the expansion of $U(y,z,t)$ and computes the eigenvalue c and the eigenfunctions. The number of terms in the expansion of $U(y,z,t)$ can be varied and is increased until the growth rates for instability do not vary significantly. Similarly, the code increases the number of terms m in the expansion of the perturbation until successive approximations to the growth rate $\mathrm{Im}(c)$ differ by less than $\approx 0.5\%$.

Figures 6 and 7 compare growth rates obtained from direct numerical simulations with those obtained from linear stability analysis for the three cases. The small circles are from direct numerical simulations, as reported in figure 5, for example. A difficulty in these computations is choosing the most appropriate streak profile. In our calculations the profiles $\{U_i\}$ are taken from the numerical simulations at times $t = 30, 60, 80$ for Couette flow and $t = 40, 70, 90$ for Poiseuille flow. We see that there is good quantitative agreement between the numerical simulation and the linear stability analysis for Couette flow and qualitative agreement for Poiseuille flow.

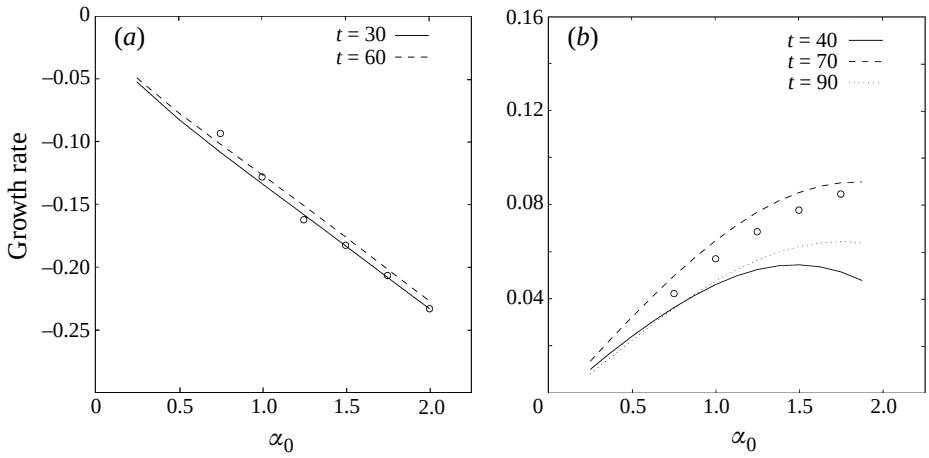

FIGURE 7. Same as figure 6 for (*a*) low-amplitude Couette and (*b*) high-amplitude Poiseuille computations.

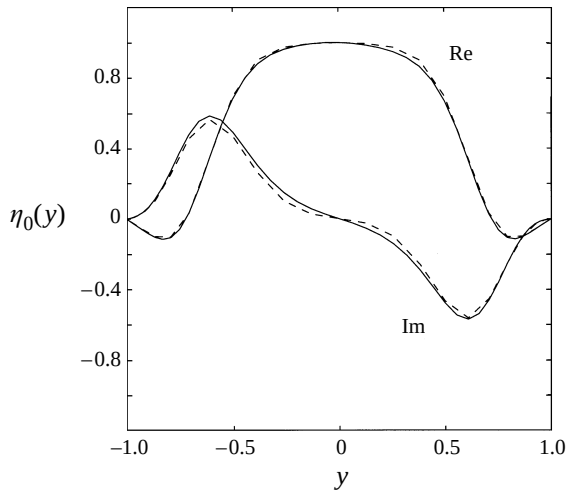

FIGURE 8. Real and imaginary parts of $\eta_0(y)$ for the least-stable mode for Couette flow (Case 2) and $\alpha_0 = 0.75$ at $t = 60$. The solid line is from the numerical simulation and the dashed line is from the linear stability analysis with $m = 6$ terms.

For the high-amplitude streaks where there is streak instability, we find that the least-stable mode is sinuous.

To verify the linear stability analysis results we did computations with 25 and 33 Chebyshev grid points in the normal y-direction. In general the computed growth rate oscillates as a function of the number of terms in the expansions of the disturbance and $U(y, z, t)$. The number of terms required for convergence increases with α_0 and the streak amplitude. For the case of low-amplitude streaks in Couette flow (Case 1) $m = 5$ terms in the expansion of the disturbance yielded converged results, independent of α_0. For the two other cases, as many as 14 terms were required for convergence. The number of terms in the expansion of $U(y, z, t)$ was 4 for Case 1, 7 for Case 2, and 9 for Case 3. These results are consistent with those of Waleffe (1995*a*), who has done an extensive convergence study.

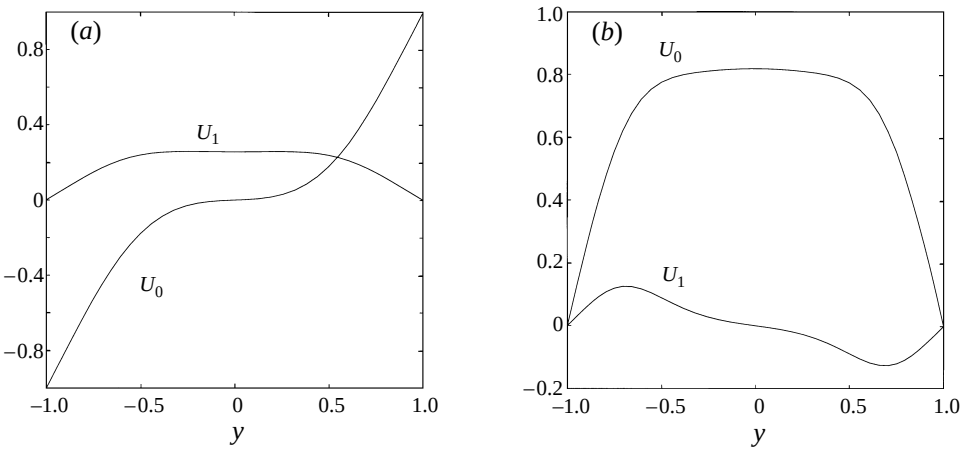

FIGURE 9. Mean flow profiles $U_0(y,t)$ and streak profiles $U_1(y,t)$ for high-amplitude streaks in (*a*) Couette ($t = 60$) (Case 2) and (*b*) Poiseuille ($t = 70$) flow (Case 3).

The eigenfunctions from linear stability analysis agree well with those from direct numerical simulations. As the streak breakdown progresses, the dominant structure in the noise modes will be the eigenfunction associated with the least-stable mode. Figure 8 compares $\eta_0(y)$ taken from the direct simulation with the eigenfunction associated with the least-stable mode computed by the linear analysis. There is good agreement for higher modes as well.

We did not determine the phase velocity of the least-stable mode in the direct numerical simulations, but we did compute it using linear stability analysis. For the perturbations given in (5), (6) the phase velocity is defined as c_r/α_0, where c_r is the real part of the eigenvalue c. We have computed the phase velocities corresponding to the growth rates in the two cases of high-amplitude streaks (Cases 2 and 3); see figures 6 and 7(*b*). For Couette flow, when the growth rate is positive the phase velocity is 0. For Poiseuille flow, the phase velocity is ≈ 0.7–0.8 for all points on the curves in figure 7(*b*), which again correspond to positive growth rates. The results for Poiseuille flow are consistent with those in Kawakami *et al.* (1997), where a phase velocity of ≈ 0.69 is found.

It appears that the phase velocity is correlated with the mean velocity $U_0(y,t)$ at the centre of the channel $y = 0$. As shown in figure 9, these velocities are 0 and ≈ 0.8 for the Couette and Poiseuille flow examples, respectively. Note that the velocity profiles are flat at the centre of the channel. Plots of the eigenfunctions indicate that the least-stable mode in cases of positive growth rate is located at the centre of the channel, as in figure 8.

It is interesting to plot the entire spectrum of the linear stability matrix. Figure 10 shows the results for Cases 2 and 3. The location of the least-stable mode changes with streak amplitude. For the laminar Couette profile, $U_0 = y$, in the absence of streaks, the least-stable modes are localized near the walls and have phase velocities $\approx \pm 1$. For laminar Poiseuille flow, the least-stable mode, a TS wave, has phase velocity ≈ 0.3 and is located near the walls, as well.

The essence of the streak breakdown can be understood by considering the stability of the purely spanwise profile

$$U(z) = A_S \cos \beta_0 z \tag{9}$$

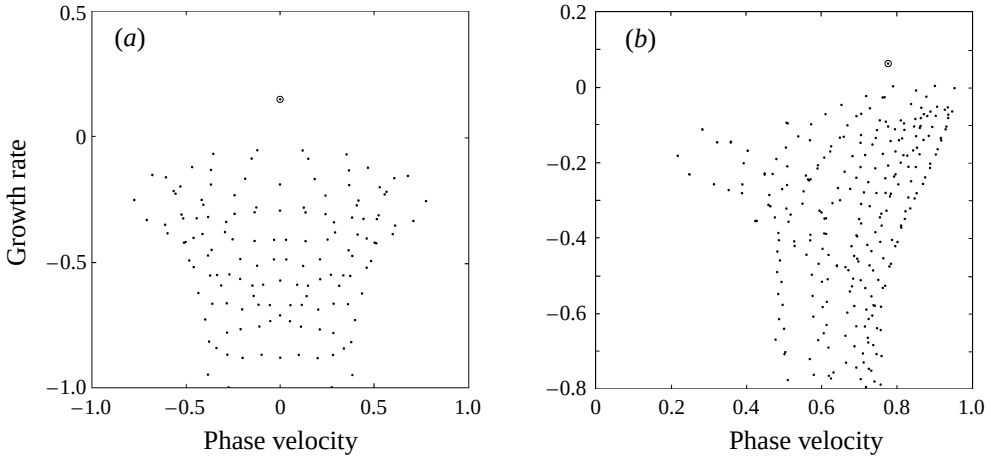

FIGURE 10. Spectra of the stability matrices for high-amplitude streaks in (*a*) Couette ($t = 60$) (Case 2) and (*b*) Poiseuille ($t = 70$) flow (Case 3). Here $\alpha_0 = 1$. The least-stable mode is circled.

to perturbations in the (x, z)-plane in inviscid flow (Finlay *et al.* 1988; Waleffe 1995*a*). Here A_S, the streak amplitude, is a constant. It is assumed that $v = 0$ and all perturbations are independent of y. For a one-term truncation, the eigenvalue is given by Waleffe (1995*a*)

$$c = \mathrm{i}\frac{|\alpha_0 A_S|}{\sqrt{2}}\left(\frac{\beta_0^2 - \alpha_0^2}{\beta_2^2 + \alpha_0^2}\right)^{1/2}. \tag{10}$$

Hence, the flow is unstable for $0 < \alpha_0 < \beta_0$ and is neutrally stable for $\alpha_0 \geqslant \beta_0$. The results are qualitatively the same if more terms are included in the expansion.

The discussion above on the model problem and the results in figures 6, 7, and previous work by other researchers suggest that the instability occurs for streamwise wavenumbers α_0 satisfying $\alpha_{min} < |\alpha_0| < \alpha_{max}$. Roughly speaking, α_{max} is on the order of β_0. For the Couette flow example (Case 2), $\alpha_{max} < \beta_0$. Direct simulations indicate that $\alpha_{max} \approx 3.5$ for the Poiseuille flow example (Case 3). For viscous flow the growth rate is negative for $\alpha_0 = 0$; in fact the growth rate is $O(R^{-1})$ for $\alpha_0 = 0$ as $R \to \infty$. Numerical simulations involving a model problem and (10) indicate that the growth rate increases linearly with α_0 for small α_0, suggesting that $\alpha_{min} = O(R^{-1})$. For Poiseuille and Couette flow we have not been able to prove this result. We conjecture that $\alpha_{min} = o(1)$ as $R \to \infty$. If there is an instability, the phase velocity of the least-stable mode is roughly equal to the mean velocity at the centre of the channel, $U_0(0, t)$.

The dependence of the growth rate on amplitude is more complicated for Poiseuille and Couette flow than it is for the inviscid model problem. For simplicity, we have decided to investigate dependence on initial vortex amplitude $A_V = 2E^{1/2}$, where E is the initial disturbance energy density. We determine the maximum growth rate as a function of time for $\beta_0 = 2$ and $\alpha_0 = 1$. Roughly speaking, if the vortex amplitude A_V is small, the streak amplitude is $|U_1| \approx CA_V R$, where C is a constant.

Results for Poiseuille flow are shown in figure 11. There are several features to note. First, there is a cusp in the graph, and this is clearly visible for the $R = 3000$ curve. For small vortex amplitude the growth rate is independent of amplitude. In this case, the flow is dominated by the mean flow $U_0(y, t)$, which is essentially the initial laminar profile $1 - y^2$. The least-stable mode for the laminar flow is a varicose mode,

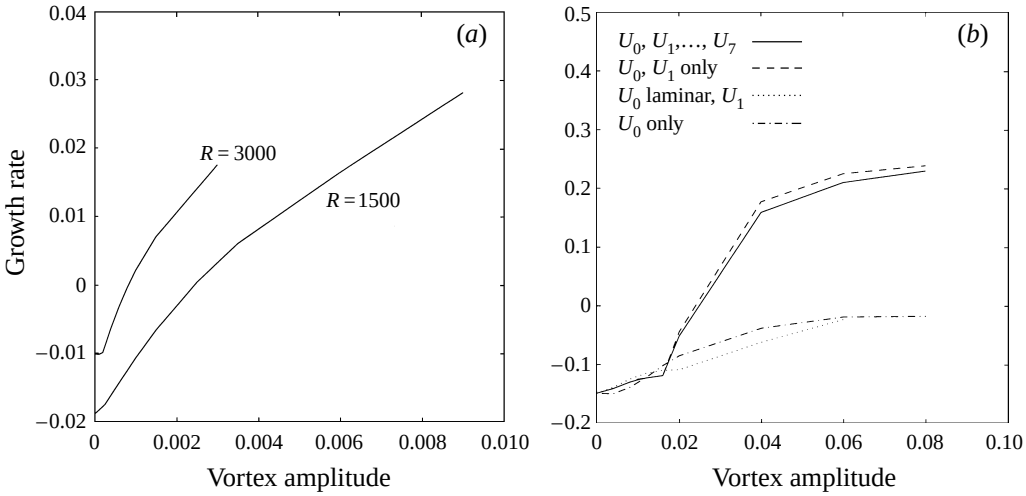

FIGURE 11. Maximum growth rate as a function of initial vortex amplitude for (*a*) Poiseuille and (*b*) Couette flow ($\alpha_0 = 1$ and $\beta_0 = 2$).

located near the wall with phase velocity of ≈ 0.3. As the initial vortex amplitude increases, the streaks become more prominent and have the predominant influence on the stability characteristics of the flow. The least-stable mode is a sinuous mode, centered near $y = 0$ with phase velocity ≈ 1.

The qualitative features of the curves in figure 11 do not change if the higher harmonics $U_2, U_3, \ldots$, are not included in the calculations or if U_0, which is modified by nonlinear interactions, is replaced by the laminar profile $1 - y^2$. As the amplitude increases, the growth rate increases. The curves are approximately straight, suggesting qualitative agreement with (10) for the model inviscid problem. The slopes of the curves are approximately 8 and 16 for Reynolds numbers 1500 and 3000, respectively. The difference in slopes is due to the fact that a vortex of amplitude A_V generates a streak with amplitude $|U_1| \approx O(A_V R)$.

Kawakami *et al.* find that growth rate increases linearly with streak amplitude and is independent of Reynolds number in their spatial experiments in plane Poiseuille flow with Reynolds number in the range 2000–2900.

Results for Couette flow for $R = 500$ are shown in figure 11(*b*). The solid curve takes into account all terms in the expansion of the streak. The dominant feature of the curve is the cusp and the rapid increase in the growth rate for amplitudes $\geqslant 0.018$. For low initial amplitudes, the least-stable modes are concentrated near the wall moving with phase velocity $\approx \pm 0.7$. For amplitudes $\geqslant 0.018$, the least-stable mode is a centre mode with phase velocity 0. Note that the cusp also exists if only U_0 and U_1 are included in the calculation. The growth rate is substantially lower if U_0 is replaced by the laminar profile y or if only the modified U_0 is included. Hamilton *et al.* (1995) have done similar calculations and find that it is the combination of the streaks and modified mean flow that is unstable. They do not report results on the stability of the streaks and the laminar Couette flow.

Coughlin (1996) has produced plots similar to those in figure 11. In her work the growth rate is determined by direct numerical simulations as a function of a forcing parameter instead of amplitude.

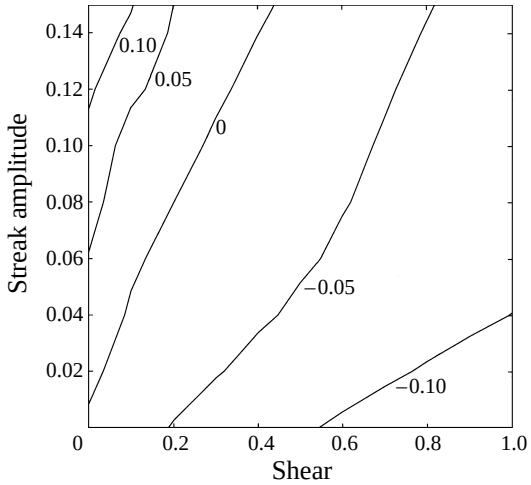

FIGURE 12. Growth rate of least-stable sinuous mode for model profile $U(y,z) = Sy + 2A_S \cos\beta_0 z$. Here $\alpha_0 = 1$ and $R = 500$.

For Couette flow streak instability depends on both the streak amplitude $|U_1|$ and the modified mean flow U_0. The key component of the mean flow is the shear $\partial U_0/\partial y$. For Couette flow in the absence of disturbances, the mean shear is 1 throughout the channel. Mean shear is reduced at the centre of the channel as streamwise vortices generate streamwise streaks. A discussion of this fact for a model problem is presented in Appendix B. For streamwise-dependent disturbances in a viscous flow, mean shear is stabilizing, since mean shear leads to increased gradients in the normal direction, thus increasing dissipation (Dubrulle & Nazarenko 1994). As a result, for example, small disturbances decay with rate $O(R^{-1/3})$ in plane Couette flow (Drazin & Reid 1981) and only $O(R^{-1})$ in flow with zero laminar velocity as $R \to \infty$.

We investigate the effects of the shear and streak amplitude on streak instability by computing growth rates for the contrived model velocity profile:

$$U(y,z) = Sy + 2A_S \mathrm{Re}\{e^{i\beta_0 z}\} = Sy + 2A_S \cos\beta_0 z,$$

where S is the shear and A_S is the streak amplitude. Figure 12 plots contours of the growth rate for the least-stable sinuous mode for $\alpha_0 = 1.0$, $\beta_0 = 2$, and $R = 500$. For fixed streak amplitude, the growth rate increases as the shear decreases. The spacing between the contour curves indicates that the increase becomes more rapid as S approaches 0. For $S = 0$, streak breakdown occurs for $A_S \geqslant 0.01$. When the shear is large streak breakdown can occur only if the streak amplitude is large. For $S = 1$, for example, a positive growth rate is achieved for $A_S \geqslant 0.42$.

The discussion above indicates that the mean shear plays a dual role in spanwise inflectional instability. On one hand, mean shear is necessary for the creation of spanwise-varying streaks, as shown in (3). On the other hand, mean shear is stabilizing. Waleffe (1997) found this to be the case as well for a four-dimensional model of a self-sustaining process in turbulent shear flows.

We end this section by examining growth rates for more general disturbances of the form

$$v(x,y,z,t) = \mathrm{Re}\{e^{i\alpha_0 x - ict} \sum_k v_k(y) e^{i(k+\sigma)\beta_0 z}\}, \tag{11}$$

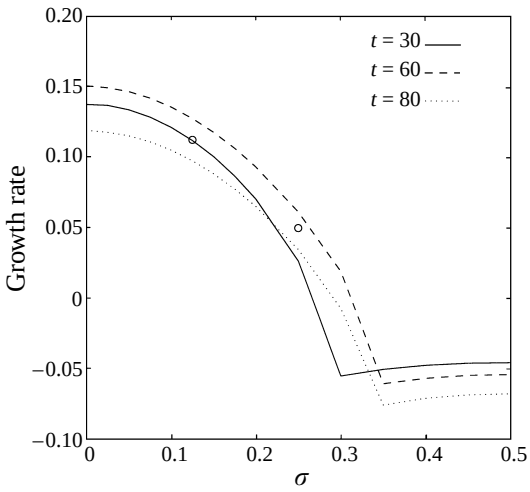

FIGURE 13. Growth rates for instability of detuned modes in high-amplitude streaks in Couette flow ($\alpha_0 = 1$). The two small circles are from numerical simulations.

$$\eta(x, y, z, t) = \mathrm{Re}\{e^{i\alpha_0 x - ict} \sum_k \eta_k(y) e^{i(k+\sigma)\beta_0 z}\}. \tag{12}$$

The constant σ is called the detuning parameter.

Figure 13 plots the growth rate as a function of σ for $\beta_0 = 2$ and $\alpha_0 = 1$ for high-amplitude streaks in Couette flow. The small circles in figure 13 are obtained from direct numerical simulations. There is good agreement between the simulations and stability analysis.

For these calculations one cannot separate the stability equations into even and odd cases. This means that for the same number of terms in the expansion of v and η the dimension of the discrete matrix problem is doubled. For this reason, we have restricted attention to low values of α_0 in the two high-amplitude examples. We have done similar calculations for high-amplitude streaks in Poiseuille flow. We have found that the greatest positive growth rates occur for $\sigma = 0$. This indicates that the streak breakdown is a fundamental-type instability.

6. Transition initiated by oblique waves

Transition initiated by oblique waves has been investigated in a number of flow geometries including plane channels, compressible and incompressible boundary layers and compressible shear layers.

In previous work Schmid & Henningson (1992) simulated oblique transition in Poiseuille flow. Their oblique waves are the least-stable modes for $\alpha = 1$ and $\beta = \pm 1$. In their calculations spanwise symmetry is preserved. Hence, the breakdown is different than that shown in the Introduction.

In our simulations of (OW) the initial condition consists of optimal oblique waves with wavenumbers $\alpha = 1$ and $\beta = \pm 1$ plus a small amount of random noise with 1% of the oblique wave energy spread over modes with wavenumbers with $\alpha = 0, \pm 1, \pm 2$ and $\beta = 0, \pm 1, \pm 2$. Spanwise symmetry is not enforced. The addition of noise enables the streaks to break down in a manner similar to that discussed in § 5.

Figure 14 plots the energy in various wavenumbers for a simulation in Poiseuille flow with $R = 1500$. The initial energy density in the oblique waves $(1, \pm 1)$ is

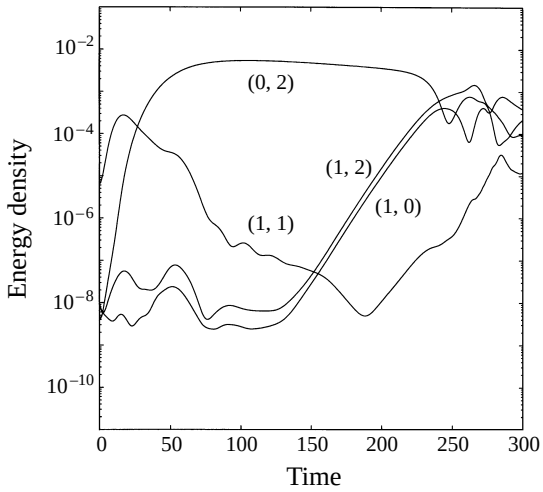

FIGURE 14. Energy density in various wavenumbers in a simulation of oblique wave transition in Poiseuille flow ($R = 1500$).

1.25×10^{-5}. The rapid growth and slow decay of energy in the $(0, 2)$ mode is similar to that for the streamwise vortex scenario. The curves for the $(1, 0)$ and $(1, 2)$ modes have the familiar signature of a secondary instability. The energy in (1,1) grows initially due to linear transient effects then decays. The growth around $t = 200$ is due to a subharmonic instability. Plots of the streamwise velocity at $t = 100$ and $t = 220$ are similar to those in figure 2.

In addition to changing the qualitative features of the transition, the addition of noise lowers the threshold for transition for the oblique wave scenario. For $R = 1500$, the threshold energy density is reduced by a factor of approximately 4.

7. Threshold amplitude for transition for (SV)

A question motivating the present paper is: how does the threshold disturbance amplitude for transition in channel flows depend on the Reynolds number? This question goes back to the early work on transition in a pipe by Reynolds.

The threshold for transition for scenario (SV) has been investigated in two recent papers by direct numerical simulations. In both papers $\beta_0 = 2$ and streamwise-dependent noise of $\approx 1\%$ of the initial disturbance energy density is added to break the symmetry. Kreiss *et al.* (1994) present examples showing that the threshold amplitude scales like R^{-1} in Couette flow for $500 \leqslant R \leqslant 4000$. A fixed streamwise vortex is used as an initial condition for all the simulations. Lundbladh *et al.* (1994) demonstrated that the threshold scales like $R^{-7/4}$ for $1500 \leqslant R \leqslant 5000$ in Poiseuille flow. The initial disturbance is the optimal streamwise vortex with initial normal velocity that is odd in y. The computations are done in a periodic box with dimensions $2\pi \times 2 \times \pi$. The computational grid is refined several times to ensure that the computed threshold value is not a numerical artifact.

For transition to take place in the above mentioned simulations, streak breakdown must occur. The growth rate for streak instability depends on the fundamental streamwise and spanwise wavenumbers. A positive growth rate for streak instability is necessary for transition but is not sufficient. In addition, whether transition occurs depends on the level of the background noise, since streaks decay slowly. In this

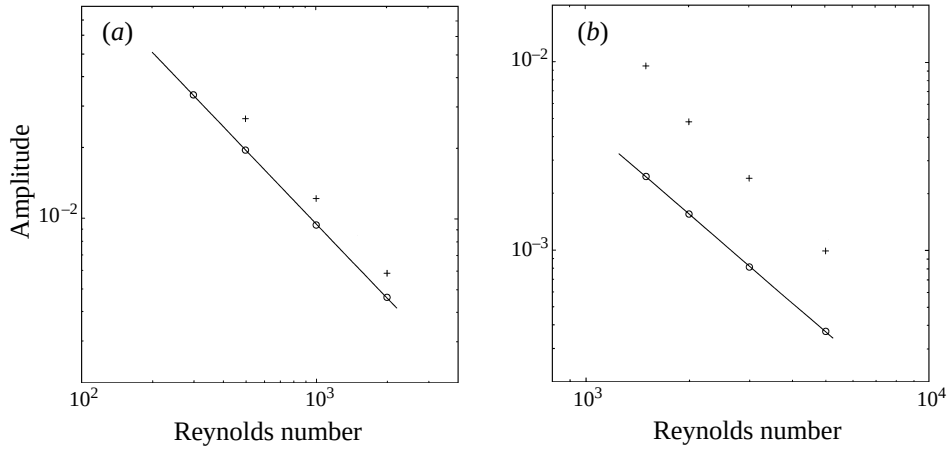

FIGURE 15. Neutral curves for streak instability for (*a*) Couette and (*b*) Poiseuille flow for $\beta_0 = 2$. The circles are computed values for the threshold vortex amplitude for a neutral growth rate, and the errors in these values are at most the size of the circles. The crosses are actual threshold vortex amplitudes for transition to turbulence from direct numerical simulations.

section we ask the question: how does the threshold amplitude for a neutral growth rate for streak breakdown depend on the Reynolds number? The threshold amplitude calculated in this section gives a lower bound for transition to turbulence, which is independent of α_0 and the level of the noise. To keep the calculations manageable, we fix $\beta_0 = 2$.

Our procedure is straightforward. For each Reynolds number we compute the optimal streamwise vortex for $\beta_0 = 2$. Streamwise streaks are generated as the vortices evolve in time. The streak profile depends on the evolution time and the amplitude of the initial vortex. For each initial vortex we determine the maximum growth rate as a function of evolution time and α_0. The neutral amplitude is the lowest amplitude for which the maximum growth rate is zero.

Figure 15 plots the neutral curve for Poiseuille and Couette flows on a log-log graph. In our calculations the amplitude is equal to two times the square root of the disturbance energy density of the initial streamwise vortex. The circles are estimated values of the threshold for a neutral growth rate. The lines are linear fits to the data. For Poiseuille flow the slope is ≈ -1.6 and for Couette flow the slope is ≈ -1. Close to the neutral amplitude in Poiseuille and Couette flows, the largest growth rate occurs for $\alpha_0 \approx 0.9$ and $\alpha_0 \approx 0.3$, respectively. The optimal time increases linearly with R in both flows. The crosses in the figure are the thresholds for transition from direct numerical simulations. The results for Poiseuille flow are from Lundbladh *et al.* (1994). The results for Couette flow are computed in a periodic box with dimensions $4\pi \times 2 \times 2\pi$ ($\alpha_f = 0.5$).

There are several reasons for the discrepancy between the threshold amplitude for transition and the threshold for a positive growth rate. First, for the growth rate calculations we have varied α_0 so that the growth rate is maximal. For the transition calculations, $\alpha_0 = 0.5$ and $\alpha_0 = 1$, for Couette and Poiseuille flow, respectively. Secondly, streamwise streaks decay with a time scale of $O(R)$ as $R \to \infty$. When the growth rate is near 0, the time scale for decay of streaks is shorter than that for streak breakdown and the linear stability analysis may not be valid. Finally, a streak instability need not result in a transition. At present, the mechanisms involved in the final phase of the transition scenario (SV) are not completely understood. The two

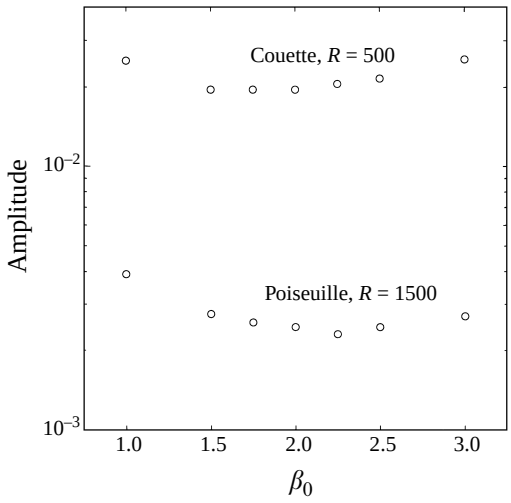

FIGURE 16. Neutral curve for streak instability as a function of the spanwise wavenumber β_0 for fixed Reynolds number.

scaling laws $R^{-1.6}$ for streak breakdown and $R^{-1.75}$ for transition in Poiseuille flow are not inconsistent, since transition can occur in principle for infinitesimal disturbance if $R > 5772$.

We have done a few computations at lower Reynolds numbers and find positive growth rates for $R = 100$ in Couette flow and $R = 750$ for Poiseuille flow. We made an initial attempt to determine the lowest Reynolds number for the streak instability in Couette flow using linear stability analysis. We found that at Reynolds number below ≈ 100 the normal and spanwise components of the streak velocity field are not negligible. The terms must be incorporated into the stability equations to get an accurate result. Using direct numerical simulations, Baggett (1996) has found that the streaks are unstable at Reynolds numbers at least as low as 50 in Couette flow and 250 in Poiseuille flow.

Figure 16 plots the threshold amplitude for breakdown of streaks as a function of β_0 for fixed Reynolds number. The minimum threshold amplitude occurs for $1.5 \leqslant \beta_0 \leqslant 2$ for Couette flow and for $2 \leqslant \beta_0 \leqslant 2.5$ for Poiseuille flow. There appears to be a correlation between the threshold vortex amplitude for streak breakdown and the potential for transient linear growth. Let $G(\beta_0, R)$ denote maximum transient linear growth factor for the optimal streamwise vortex with spanwise wavenumber β_0. For example, for Couette flow with $R = 500$ and $\beta_0 = 2$, this factor is ≈ 15. This means that a vortex with 'amplitude' ϵ can evolve into a streak with amplitude 15ϵ in a linear calculation. Growth rates for streak breakdown depend on streak amplitude. This suggests that the minimum threshold for transition should approximately occur for that wavenumber with the greatest potential for transient linear growth. This appears to be the case, since the greatest potential for linear growth occurs for $\beta_0 \approx 1.67$ and ≈ 2.6 in Couette and Poiseuille flow, respectively.†

† For Poiseuille flow the potential for transient growth is greatest for initial streamwise vortices that are even with respect to y. For these disturbances, the greatest transient growth occurs for $\beta_0 \approx 2$. It turns out that the threshold amplitude for transition to turbulence is lower for initial streamwise vortices that are anti-symmetric with respect to y. For these disturbances, the greatest growth occurs for $\beta_0 \approx 2.6$.

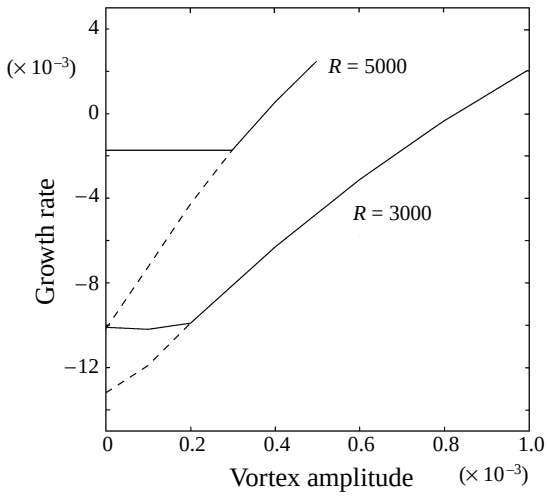

FIGURE 17. Growth rate versus initial vortex amplitude for Poiseuille flow $\alpha_0 = 1$ and $\beta_0 = 2$. The solid line is for the least-stable mode. The dashed line is the growth rate for the least-stable sinuous mode.

The scaling result for Poiseuille flow can be explained in a straightforward manner. Roughly speaking, streak breakdown occurs if the spanwise inflectional instability is sufficiently strong to overcome dissipation. Figure 17 plots growth rate versus vortex amplitude. Let us explain the plot by focusing on the $R = 5000$ curves. Except for small vortex amplitudes $\leqslant 3 \times 10^{-3}$, where the varicose mode is dominant, the least-stable mode is a sinuous mode. The dashed line is the growth rate of the least-stable sinuous mode for small amplitudes. For the relevant range of vortex amplitudes the growth rate increases linearly with vortex amplitude; we have

$$\gamma \approx -D(R) + CA_V R, \tag{13}$$

where A_V is the vortex amplitude, C is a positive constant, and $D(R)$ is the dissipation term. Here we assume α_0 is fixed.

The key question is: what is $D(R)$? This quantity is the decay rate of the sinuous mode in laminar Poiseuille flow. The least-stable mode for laminar Poiseuille flow lies on the A branch of the spectrum. It is this mode which is unstable when the Reynolds number is sufficiently large. The least-stable *sinuous* mode lies on the P branch of the spectrum. The modes on the P branch are stable for all R. Numerical computations of growth rates shows that the least-stable P mode has a growth rate of $D(R) \approx C'R^{-0.55}$, where C' is a constant.

Solving (13) for A_V when $\gamma = 0$ it follows that that the threshold amplitude satisfies $A_V \approx C''R^{-1.55}$, consistent with the results in figure 15.

The same heuristic argument is also valid for two model problems. Consider (*a*) $U(y,z) = 2A_S(1-y^2)\cos 2z$ and (*b*) $U(y,z) = 1-y^2+2A_S(1-y^2)\cos 2z$. For case (*a*), no mean flow, computations show that the threshold streak amplitude for breakdown scales like C_1R^{-1} as $R \to \infty$. For (*b*), where the mean flow is laminar Poiseuille flow, the threshold scales like $C_2R^{-0.55}$. The growth rate for low amplitudes satisfies $\gamma \approx -D(R) + CA_S$, where C is a constant, for low streak amplitudes. For the case of no flow $D(R) = O(R^{-1})$ as $R \to \infty$, corresponding to pure diffusion, and this yields

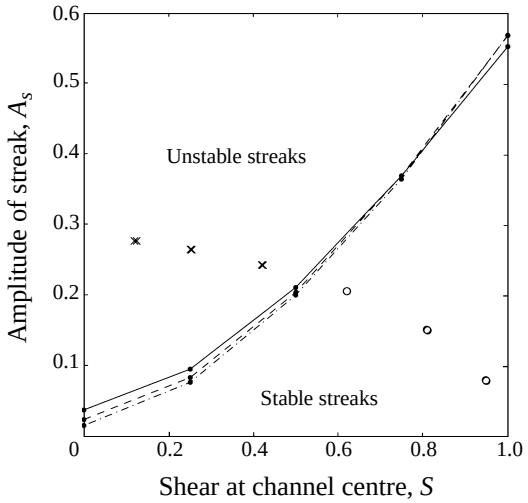

FIGURE 18. Neutral stability curves for the model Couette flow model problem of this section. The three curves from bottom to top at $S = 0$ correspond to $R = 2000, 1000, 500$. The circles and crosses correspond to measurements of the shear and centreline amplitude of stable and unstable streaks, respectively, from actual simulations. There are three circles or three crosses at each position corresponding to three actual streaks generated from optimal vortices of amplitude $\epsilon, \epsilon/2, \epsilon/4$ at $R = 500, 1000, 2000$, respectively.

the threshold result $A_S = O(R^{-1})$ as $R \to \infty$, agreeing with computations. For (*b*), $D(R) \approx C'R^{-0.55}$, and we get the result $A_S \approx C''R^{-0.55}$.

Unlike Poiseuille flow, in Couette flow an $O(1)$ streak and/or an $O(1)$ shear reduction, independent of R, is required for the streaks to be linearly unstable. To generate such streaks or shear reduction the initial streamwise vortices must have amplitude $O(R^{-1})$ (see Appendix B). This behaviour is consistent with that in the four-dimensional system of ordinary differential equations proposed by Waleffe (1997) as a model of a self-sustaining turbulent cycle in shear flows.

The simple model problem considered in § 5 does not capture the $O(R^{-1})$ threshold amplitude, so we instead consider the more physical model velocity profile (Baggett 1996):

$$\begin{aligned} U(y,z) &= y + U_0(y) + U_1(y)\cos\beta_0 z \\ &= Sy + (S-1)(-2y^3 + y^5) + A_S(1-y^2)\cos\beta_0 z. \end{aligned} \tag{14}$$

The profiles are chosen such that the mean flow is an S-shaped curve and the y-dependence of the streak is parabolic to mimic the profiles in actual simulations such as those shown in figure 9. Comparisons of the model profiles and profiles from simulations can be found in Baggett (1996). The parameter S determines the shear at the channel centre and parameter A_S determines the streak amplitude. Figure 18 shows the neutral stability curves for $\alpha_0 = 1$, $\beta_0 = 2$, and $R = 500$, 1000 and 2000. Except for small S these curves are fairly independent of R and they all lie at a constant distance from the laminar solution $(S, A_S) = (1, 0)$ in the lower right corner of the figure. To verify that the neutral stability curves for the model profile agree with the neutral stability of streaks generated from optimal streamwise vortices we have plotted measurements of $\partial U_0(0, t_{max})/\partial y$ and $|U_1(0, t_{max})|$ from direct numerical simulations, where t_{max} is the time at which the streak instability growth rate is largest. In each simulation the stability of the streaks is predicted by the stability of the model

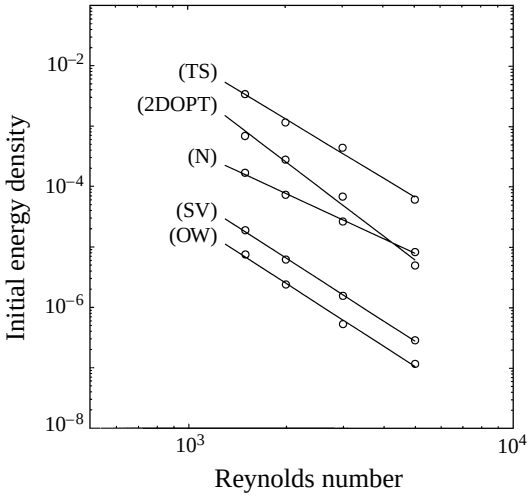

FIGURE 19. Threshold energy density for transition in Poiseuille flow for the three main scenarios, two-dimensional optimals (2DOPT), and random three-dimensional noise (N). The circles correspond to data from simulations. The lines are fits to the data.

profile. In fact, each circle or cross represents three independent simulations where the streaks are generated by initial streamwise vortices of amplitude $\epsilon, \epsilon/2, \epsilon/4$ for $R = 500, 1000, 2000$, respectively.

8. Comparison of thresholds for transition

How do the thresholds for transition compare for the secondary instability scenario, the streamwise vortex scenario, and the oblique wave scenario?

Figure 19 plots the threshold energy density for transition for the three scenarios for Poiseuille flow for $1500 \leqslant R \leqslant 5000$. We have also computed a threshold for transition initiated by two-dimensional optimal disturbances (2DOPT) (Farrell 1988). These optimals have potential for moderate linear transient growth – a factor of $O(10)$ – at subcritical Reynolds numbers. As in the (TS) scenario, these initial conditions also evolve into two-dimensional states that are linearly unstable to three-dimensional disturbances. Finally, we compute a threshold for noise consisting of a random combination of Stokes modes with streamwise and spanwise wavenumbers $0, \pm 1, \pm 2$ (N). The threshold transition energy for scenarios (SV) and (OW) is more than two orders of magnitude below that for (TS) and more than one order of magnitude lower than that for two-dimensional optimals.

The procedure to create the plot is straightforward. For each scenario we run the full nonlinear simulation code with initial disturbances of varying energy density. We obtain upper and lower bounds on the initial energy for transition and have plotted the average of these values. For scenarios (TS), (2DOPT), (SV) and (OW) noise with energy density of 1% of the principal disturbance energy is added. We have verified our results by increasing the resolution of the computational grid. The results are listed in tables 2 and 3. The upper and lower bounds on the threshold energy listed include the noise. For scenario (SV) the initial streamwise vortex has $\beta_0 = 2$. For scenario (OW) the oblique waves have $\alpha_0 = 1$ and $\beta_0 = \pm 1$. For (TS) the initial TS wave has $\alpha_0 = 1$. For (2DOPT) the optimal disturbance for $\alpha_0 = 1$ and $\beta_0 = 0$ is used.

Scenario	R	Grid	Lower	Upper
(SV)	1500	$16 \times 81 \times 64$	1.83×10^{-5}	1.93×10^{-5}
	2000	$16 \times 81 \times 64$	6.32×10^{-6}	6.64×10^{-6}
	3000	$16 \times 81 \times 64$	1.46×10^{-6}	1.52×10^{-6}
	5000	$16 \times 81 \times 64$	2.56×10^{-7}	2.65×10^{-7}
(OW)	1500	$16 \times 81 \times 48$	7.28×10^{-6}	7.67×10^{-6}
	2000	$16 \times 81 \times 64$	2.33×10^{-6}	2.43×10^{-6}
	3000	$16 \times 81 \times 64$	5.03×10^{-7}	5.53×10^{-7}
	5000	$16 \times 81 \times 64$	1.14×10^{-7}	1.19×10^{-7}
(TS)	1500	$32 \times 81 \times 64$	3.30×10^{-3}	3.45×10^{-3}
	2000	$32 \times 81 \times 64$	1.11×10^{-3}	1.18×10^{-3}
	3000	$32 \times 81 \times 64$	4.31×10^{-4}	4.50×10^{-4}
	5000	$32 \times 81 \times 64$	5.75×10^{-5}	6.45×10^{-5}
(N)	1500	$32 \times 81 \times 64$	1.65×10^{-4}	1.70×10^{-4}
	2000	$32 \times 81 \times 64$	7.00×10^{-5}	7.50×10^{-5}
	3000	$32 \times 81 \times 64$	2.50×10^{-5}	2.75×10^{-5}
	5000	$40 \times 97 \times 80$	8.50×10^{-6}	8.75×10^{-6}
(2DOPT)	1500	$32 \times 81 \times 64$	6.66×10^{-4}	6.99×10^{-4}
	2000	$32 \times 81 \times 64$	2.67×10^{-4}	2.88×10^{-4}
	3000	$32 \times 81 \times 64$	6.66×10^{-5}	6.95×10^{-5}
	5000	$32 \times 81 \times 64$	4.81×10^{-6}	5.09×10^{-6}

TABLE 2. Upper and lower bounds on the threshold energy density for transition for the five scenarios in Poiseuille flow. The results are given for the most refined grid. For scenario (SV) the computational box is of size $2\pi \times 2 \times \pi$ ($\alpha_f = 1$ and $\beta_f = 2$). For the four other scenarios it is size $2\pi \times 2 \times 2\pi$.

Scenario	R	Grid	Lower	Upper
(SV)	500	$16 \times 81 \times 64$	1.92×10^{-4}	1.96×10^{-4}
	1000	$16 \times 81 \times 64$	3.50×10^{-5}	3.65×10^{-5}
	2000	$16 \times 81 \times 64$	8.53×10^{-6}	8.66×10^{-6}
(OW)	500	$16 \times 81 \times 64$	6.49×10^{-5}	6.61×10^{-5}
	1000	$16 \times 81 \times 64$	1.20×10^{-5}	1.21×10^{-5}
	2000	$16 \times 81 \times 64$	2.14×10^{-6}	2.18×10^{-6}
(N)	500	$32 \times 81 \times 64$	2.75×10^{-3}	3.00×10^{-3}
	1000	$32 \times 81 \times 64$	2.25×10^{-4}	2.50×10^{-4}
	2000	$32 \times 81 \times 64$	3.60×10^{-5}	4.00×10^{-5}

TABLE 3. Upper and lower bounds on the threshold energy density for transition for three scenarios in Couette flow The results are given for the most refined grid. For scenario (SV) the computational box is of size $4\pi \times 2 \times \pi$ ($\alpha_f = 0.5$ and $\beta_f = 2$). For the other two scenarios it is size $2\pi \times 2 \times 2\pi$.

Except for $R = 3000$ and $R = 5000$ for scenario (N), the upper and lower bounds are the same on the next most refined grid, which has resolution $12 \times 65 \times 48$ or $24 \times 65 \times 48$.

There are several methods of determining if transition has taken place. For example, one can look for sharp peaks in the energy density or in the Reynolds number based

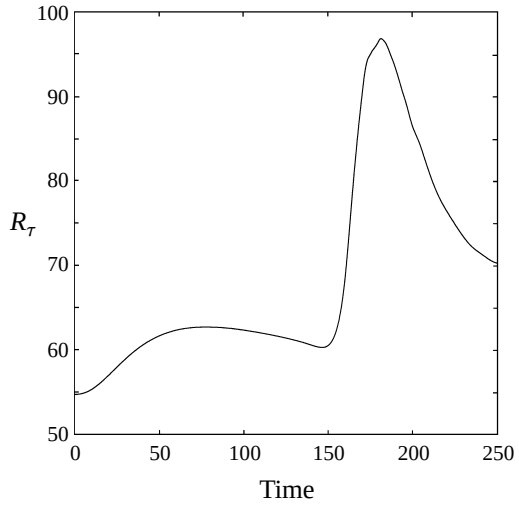

FIGURE 20. Reynolds number based on friction velocity for a simulation of scenario (SV) in Poiseuille flow with $R = 1500$. In this case the initial disturbance energy is 2×10^{-4}, which is about twice the threshold value.

on friction velocity at the wall. The friction velocity is defined as

$$U_\tau = \left(\nu \left. \frac{\partial U}{\partial y} \right|_{wall} \right)^{1/2}.$$

A typical plot of the Reynolds number based on friction velocity is shown in figure 20 for a simulation of (SV). There is a slow increase in R_τ as vortices generate streaks, then a rapid increase to peak, as the streaks break down and transition occurs. In the cases where transition occurs we have not verified that a turbulent state is sustained.

For the (TS) and (2DOPT) scenarios the fundamental wavenumbers are $\alpha_f = \beta_f = 1$ and the initial TS wave has streamwise wavenumber $\alpha_0 = 1$. For our simulations only a fundamental-type breakdown is permitted. If subharmonic-type breakdown is allowed, then we find that the threshold is marginally lower. For example for the (TS) scenario for $R = 1500$ the threshold drops from $\approx 3.4 \times 10^{-3}$ to 3×10^{-3}.

Although (SV) and (OW) have lower thresholds than (TS) and (2DOPT), the former scenarios occur on a time scale $O(R)$, whereas (TS) and (2DOPT) occur on a time scale $O(1)$. The $O(R)$ originates from the fact that this is the time scale in which streaks are generated from streamwise vortices. We investigate transition time as a function of initial disturbance energy for the five scenarios. We define transition time as the time when the Reynolds number based on the friction velocity reaches the value halfway between its initial laminar value and the value at the transition peak. If transition does not occur the transition time is defined to be ∞.

Transition times as a function of the initial disturbance energy for $R = 1500$ and $R = 5000$ are shown in figure 21. It is indeed the case that transition occurs on a viscous time scale for scenarios (SV) and (OW) if the disturbance energy is the near the threshold value. As the disturbance energy increases, the transition time decreases significantly. For $R = 1500$, if one considers transition at comparable times, the threshold for (SV) is an order of magnitude lower than for (TS) and a factor of about three lower than for (2DOPT). The threshold for (OW) is two orders of

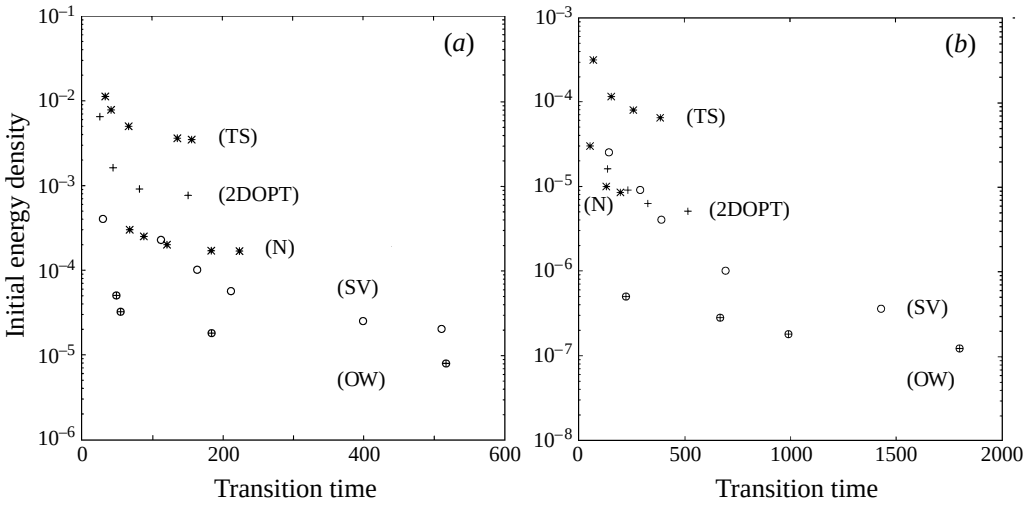

FIGURE 21. Transition time as a function initial disturbance energy density in Poiseuille flow (*a*) $R = 1500$ and (*b*) $R = 5000$. The symbols are: $*$, Tollmien-Schlichting (TS); $+$; 2D optimals (2DOPT); $*$ Noise (N); $\circ$ streamwise vortices (SV); $\oplus$ oblique waves (OW).

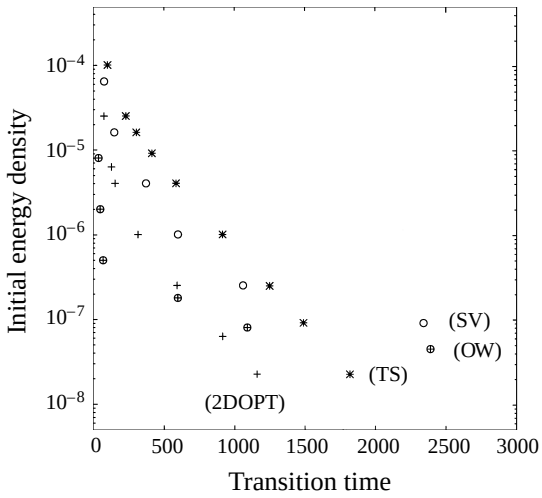

FIGURE 22. Transition time as a function initial disturbance energy density in Poiseuille flow ($R = 7500$). The symbols are as in figure 21.

magnitude lower than that of (TS) and more than an order of magnitude lower than that of (2DOPT).

As the Reynolds number increases to $R = 5000$, (TS) and (2DOPT) become more competitive with (SV). The difference in the threshold between (TS) and (SV) is only a factor of ≈ 4 for transition occurring at time 150. The (2DOPT) scenario has a lower threshold than (SV) for transition at early times. The (OW) has a threshold that is still substantially lower than that for (TS) and (2DOPT).

At supercritical Reynolds numbers transition can be initiated by scenarios (TS) and (2DOPT) by an infinitesimal disturbance, since the flow is linearly unstable. Figure 22 shows that if the initial energy density is less than $\approx 6 \times 10^{-8}$, then transition via (TS) occurs earlier than via (SV) and (OW). The (2DOPT) scenario undergoes

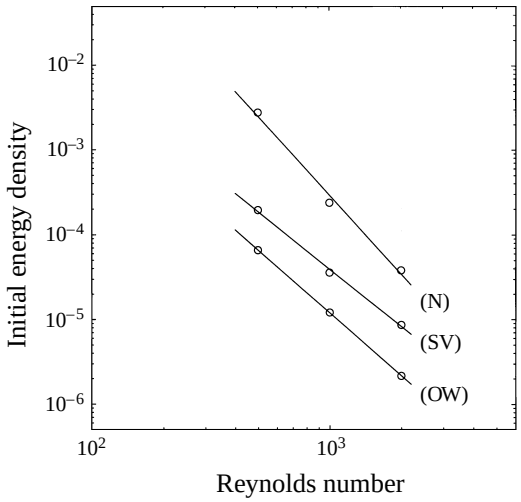

FIGURE 23. Threshold energy density for transition in Couette flow.

transition earlier than (SV) for all initial energies. If the initial energy is lower than $\approx 10^{-7}$, then (2DOPT) 'beats' (OW) as well.

Figure 23 plots the threshold energy density for transition in Couette flow. As in the case of Poiseuille flow, the (OW) scenario has the lowest threshold. For the data collected, the threshold energy density scales like approximately $R^{-2.2}$, $R^{-2.5}$, $R^{-3.1}$ for the streamwise vortex, oblique wave, and noise scenarios respectively. The result for (SV) corresponds to a threshold amplitude exponent of -1.1, which is close to exponent of ≈ -1 found for streak breakdown.

Extrapolating the curves in figure 23, it appears that the threshold for the noise scenario could be smaller than that for (SV) and (OW) when the Reynolds number is sufficiently large. We plan on investigating this further in future work.

9. Discussion

We have investigated streak instability, a Kelvin–Helmholtz-like instability in plane Couette and Poiseuille flow. This type of breakdown has been investigated in detail in other flow geometries. For channel flows the instability has the following properties.

(*a*) Instability occurs for perturbations with streamwise wavenumbers α_0 satisfying $0 < \alpha_{min} < |\alpha_0| < \alpha_{max}$. Roughly speaking α_{max} is on the order of β_0, the spanwise wavenumber of the streak, and it is conjectured that $\alpha_{min} = o(1)$ as the Reynolds number increases to ∞.

(*b*) The growth rate for streak breakdown increases with streak amplitude.

(*c*) In cases of a positive growth rate, the least-stable mode is located at the centre of the channel and has phase velocity approximately equal to the mean velocity at the centre of the channel.

(*d*) Streak breakdown is inhibited by mean shear at the centre of the channel. This phenomenon is relevant in Couette flow, where the mean shear of the laminar profile is 1. Streak breakdown occurs when the streak amplitude is sufficiently large to overcome the stabilizing effects of mean shear. Due to the importance of shear in the normal direction the streak breakdown cannot be completely characterized as a two-dimensional Kelvin–Helmholtz instability.

(*e*) For the parameter combinations considered in this paper, we find that streak breakdown in channel flows is a fundamental-type instability.

(*f*) We find that threshold vortex amplitude for instability scales like $R^{-1.6}$ for $1500 \leqslant R \leqslant 5000$ in Poiseuille flow and like R^{-1} for $300 \leqslant R \leqslant 2000$ in Couette flow. The scaling result for Poiseuille flow can be explained straightforwardly by balancing viscous dissipation with the growth rate for streak instability in the inviscid case. For Couette flow, roughly speaking, a streak amplitude and/or a shear reduction of $O(1)$ is required for streak breakdown. A streamwise vortex with amplitude $O(R^{-1})$ is required to create such conditions.

Streak instability is a fundamental phase of transition initiated by streamwise vortices, scenario (SV), and oblique waves, scenario (OW). The threshold energy for transition in Poiseuille flow at subcritical Reynolds numbers for these scenarios is at least two orders of magnitude lower than that for transition initiated by Tollmien–Schlichting waves, scenario (TS), and an order of magnitude lower than that for transition initiated by two-dimensional optimals, scenario (2DOPT). Even the threshold for transition initiated by random noise is lower than that for (TS). The time scale for scenarios (SV) and (OW) is longer than those for (TS) and (2DOPT). However, as the initial disturbance energy is increased the time for transition for scenarios (SV) and (OW) decreases rapidly. When transition time is taken into account, our results show that the threshold energy required for transition at a given time for (SV) and (OW) is lower than that for (TS) and (2DOPT) $R = 1500$. As the Reynolds number increases to $R = 5000$, (2DOPT) and (TS) become more competitive with the (SV) scenario. The (OW) scenario has the lowest threshold at a given time; it is at least an order of magnitude lower than that for (2DOPT) and two orders of magnitude lower than that for (TS) for for $R = 1500$ and $R = 5000$. The (TS) and (2DOPT) become more competitive at supercritical Reynolds numbers.

The (TS) scenario is competitive with (SV) and (OW) in the temporal boundary layer (Schmid, Reddy & Henningson 1996). In the temporal boundary layer the Reynolds number increases in the downstream direction. In calculations done in that geometry, scenario (OW) has the lowest threshold, followed by (TS) and (SV). This is consistent with results of Chang & Malik (1994), who find that the threshold amplitude for scenario (OW) in a supersonic boundary layer is two orders of magnitude lower than that for (TS).

Streak breakdown is necessary but not sufficient for transition to occur in scenarios (SV) and (OW). A goal of future work is to investigate the final stages of transition in these scenarios. A lead in this direction may be provided by recent work by Hamilton *et al.* (1995), who present a model of a self-sustaining cycle in turbulent channel flow. This cycle consists of streak formation from streamwise vortices, streak breakdown and vortex regeneration from the direct nonlinear interaction of the streak instability eigenmode. They conclude that the time scales for the various phase must match for self-sustainment.

A question that we have not addressed to this point is: Which scenario is most likely to take place at subcritical Reynolds numbers? In general, disturbances are random and not in the form of optimal streamwise vortices, oblique waves, Tollmien–Schlichting waves, or optimal two dimensional disturbances. What mechanisms describe transition at subcritical Reynolds numbers initiated by random noise? Answer to these questions are beyond the scope of the present paper.

The noise scenario was investigated previously by Kim & Moser (1989), who considered transition in Poiseuille flow at $R = 10\,000$. At this Reynolds number, theory predicts that the subharmonic-type instability of the (TS) scenario is more dominant

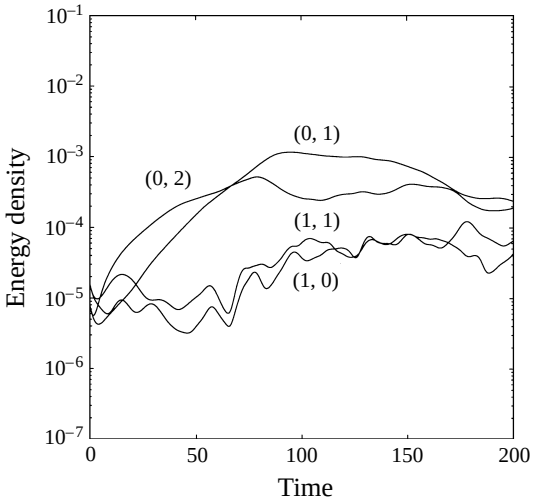

FIGURE 24. Energy in spanwise, streamwise, and oblique components in a simulation of transition initiated by random noise. Initially there is energy in the modes with $|\alpha| \leqslant 2$ and $|\beta| \leqslant 2$. The initial energy density is 2×10^{-4} and transition occurs at $t \approx 100$.

than the fundamental-type instability. However, in experiments the fundamental-type instability is found to dominate. The purpose of their paper was to explain the discrepancy between theory and experiment. They found that the initial stages of transition were explained by linear theory. The energy in the streamwise mode $(1,0)$ increased due to the linear instability and was the dominant contribution to the total energy. The energy in the spanwise modes initially increased due to transient effects, then decayed slowly. At a later time, $t \approx 2500$, they found exponential growth in the fundamental instability modes. They found that nonlinear interactions between the spanwise modes and the streamwise mode $(1,0)$ was responsible for the dominance of the fundamental-type instability over the subharmonic-type instability. A similar conclusion is reached by Singer, Reed & Ferziger (1989).

The situation appears to be different at subcritical Reynolds numbers. Figure 24 plots the energy in streamwise, spanwise, and oblique components in a simulation of transition initiated by random noise in Poiseuille flow at $R = 1500$. In this simulation transition occurs at $t \approx 100$. In contrast to the case of $R = 10\,000$, the the energy in the spanwise modes is significantly greater than that in $(1,0)$, the linearly unstable mode, at early times.

The results in figure 24 suggest that the breakdown in the random noise scenario may be similar to the (SV) scenario. However, examining the energy in $(1,0)$ and $(1,1)$ and looking at the flow fields, one cannot conclude that a pure streak breakdown as discussed in this paper takes place. We have performed preliminary computations to determine the contributions to the rate of change of energy in the spanwise mode $(0,1)$. The expression for rate of change of energy consists of a linear interaction term (with the laminar profile), a modified mean flow interaction term (with the modified flow in $(0,0)$), and nonlinear interaction terms with other modes (Schmid & Henningson 1995). For scenario (SV), the main contribution to the rate of change of energy before streak breakdown comes from the linear interaction terms. For the noise scenario above, the main contribution until $t \approx 20$ comes from the the linear and mean flow modification terms. However after $t \approx 20$, the nonlinear interaction terms

dominate. Hence, nonlinear effects come into play much earlier than in the streamwise vortex scenario. This is not surprising, since various modes have a relatively large amount of energy initially. Further work is required to understand transition initiated by random noise.

We would like to thank Hendrik Alfredsson, Håkan Gustavsson, Anne Trefethen, Nick Trefethen, Fabian Waleffe for their contributions and comments on the manuscript. We also thank the referees. S. C. R. and P. J. S. gratefully acknowledge the hospitality and support of Dan Henningson and the Department of Mechanics, Royal Institute of Technology in Stockholm, where part of this work was done. P. J. S. was supported in part by NSF grant DMS-9406636. J. S. B. was supported in part by NSF grant DMS-950090-75CS and DOE grant DE-FG02-94ER25199. Some computations were done at the Pittsburgh Supercomputing Center.

Appendix A

To study the stability of the streak we substitute $\boldsymbol{U}+\boldsymbol{u}$, where $\boldsymbol{u}(x, y, z, t) = (u, v, w)$ is the perturbation velocity and $\boldsymbol{U}$ is the streak profile, into the Navier–Stokes equations. The resulting equations, given as equation (17) in Waleffe (1995*a*), are

$$u_x + v_y + w_z = 0, \tag{A 1}$$

$$u_t + Uu_x + U_y v + U_z w = -p_x + \frac{1}{R}\Delta u, \tag{A 2}$$

$$v_t + Uv_x = -p_y + \frac{1}{R}\Delta v, \tag{A 3}$$

$$w_t + Uw_x = -p_z + \frac{1}{R}\Delta w. \tag{A 4}$$

Here, $p = p(x, y, z, t)$ is the perturbation pressure. We reduce the above equations to two equations by expressing the perturbation quantities in terms of the normal velocity v and the normal vorticity $\eta = u_z - w_x$. The manipulations are similar to those in the derivation of the Orr–Sommerfeld and Squire equations:

$$\eta_t + U\eta_x - U_z v_y + U_{yz} v + U_y v_z + U_{zz} w = \frac{1}{R}\Delta\eta, \tag{A 5}$$

$$\Delta v_t + U\Delta v_x + U_{zz} v_x + 2U_z v_{xz} - U_{yy} v_x - 2U_z w_{xy} - 2U_{yz} w_x = \frac{1}{R}\Delta\Delta v. \tag{A 6}$$

The boundary conditions are $v(y = \pm 1) = (\partial v/\partial y)(y = \pm 1) = \eta(y = \pm 1) = 0$. The spanwise velocity w can be eliminated from the above equations using the identity

$$w_{xx} + w_{zz} = -\eta_x - v_{yz}. \tag{A 7}$$

Appendix B

We present a back-of-the-envelope-type calculation showing that an initial streamwise vortex with normal velocity $\|V_1\| \approx \epsilon$ modifies the mean shear by a factor $\approx C\epsilon^2 R^2$ in time $t = O(R)$ as $R \to \infty$, where C is a constant. (See also Waleffe 1995*b*). In this Appendix we define $\|\cdot\|$ by

$$\|U\| = \sup_{-1 \leqslant y \leqslant 1} |U(y)|.$$

We consider the evolution of a streamwise vortex in a shear flow and its effect on the mean flow. To this end, we assume that the velocity field has the form

$$\begin{aligned} U(x,y,z,t) &= \overline{U}(y) + U_0(y,t) + U_1(y,t)\cos(\beta_0 z), \\ V(x,y,z,t) &= V_1(y,t)\cos(\beta_0 z), \\ W(x,y,z,t) &= W_0(y,t) + W_1(y,t)\sin(\beta_0 z) \\ P(x,y,z,t) &= \overline{P}(x) + P_0(y,t) + +P_1(y,t)\cos(\beta_0 z). \end{aligned}$$

The above expressions are truncated versions of the actual expansions used in the direct numerical simulation in § 4 and all quantities are real. The overlined quantities correspond to the laminar flow. The term $U_0(y,t)$ is the mean flow modification. It can be shown that $V_0(y,t) = 0$ and that $W_1 = -(1/\beta_0)\partial V_1/\partial y$ by applying the conservation-of-mass condition.

We substitute the above expressions for the velocity and pressure into the Navier–Stokes equations and write the result in the form of a truncated Fourier series. The equation for U_0 is obtained from the constant term in the series

$$\begin{aligned} \frac{\partial U_0}{\partial t} &= -\frac{1}{2}V_1\frac{\partial U_1}{\partial y} + \frac{\beta_0}{2}W_1U_1 + \frac{1}{R}\frac{\partial^2 U_0}{\partial y^2}, \\ &= -\frac{1}{2}V_1\frac{\partial U_1}{\partial y} - \frac{1}{2}\frac{\partial V_1}{\partial y}U_1 + \frac{1}{R}\frac{\partial^2 U_0}{\partial y^2}, \\ &= -\frac{1}{2}\frac{\partial}{\partial y}(U_1V_1) + \frac{1}{R}\frac{\partial^2 U_0}{\partial y^2}. \end{aligned} \tag{B 1}$$

Let us consider the evolution from $t = 0$ to $t = O(R)$. Streamwise velocity is created by the lift-up mechanism. In the case of a linear evolution in inviscid flow, $V_1(y,t)$ is constant and (Ellingsen & Palm 1975)

$$U_1(y,t) = U_1(y,0) - U'(y)V_1(y,t)t.$$

If viscosity is included in the calculation, then $V_1(y,t)$ decays with rate $O(1/R)$ as $R \to \infty$ and the growth in the streamwise velocity is shut off at $t = O(R)$ (Gustavsson 1991; Butler & Farrell 1992; Trefethen *et al.* 1993). Let us assume that $\|V_1\| \approx \epsilon$. From the above equation it follows that $\|U_1\| \approx \epsilon t$. Here we assume that $U_1(y,0)$ is small compared to the production term and that the laminar shear does not change significantly. Hence, we have $\|U_1V_1\| \approx \epsilon^2 t$. We assume that the normal derivative of U_1V_1 is also $\approx \epsilon^2 t$ since $U_1V_1 = 0$ at the boundaries. (We assume that there are no sharp gradients in U_1V_1.) Integrating (B 1) (ignoring the dissipation term), we have

$$\|U_0(\cdot, t = O(R))\| \approx \int_0^{O(R)} \epsilon^2 t \mathrm{d}t \approx C'\epsilon^2 R^2.$$

Finally, taking the derivative and using the fact that $U_0 = 0$ is zero at the boundaries, we conclude that

$$\left\| \frac{\partial U_0}{\partial y} \right\| \approx C\epsilon^2 R^2. \tag{B 2}$$

We have done numerical simulations with $R = 500$ and $R = 1000$ to verify the above estimate. We find that the result is approximately valid for a wide range of values of $\epsilon^2 R^2$; the constant C only decreases by $\approx 20\%$ as $\epsilon^2 R^2$ increases from 0 to 100.

REFERENCES

Baggett, J. S. 1996 Non-normal dynamics and applications in hydrodynamic stability. PhD Thesis, Cornell University.

Bakchinov, A. A., Grek, G. R., Klingmann, B. G. B. & Kozlov, V. V. 1995 Transition experiments in a boundary-layer with embedded streamwise vortices. *Phys. Fluids* A **7**, 820–832.

Bayly, B. J., Orszag, S. A. & Herbert, T. 1988 Instability mechanisms in shear flow transition. *Ann. Rev. Fluid Mech.* **20**, 359–391.

Berlin, S., Lundbladh, A. & Henningson, D. S. 1994 Spatial simulations of oblique transition. *Phys. Fluids* A **6**, 1949–1951.

Boberg, L. & Brosa, U. 1988 Onset of turbulence in a pipe. *Z. Naturforschung* **43a**, 697–726.

Butler, K. M. & Farrell, B. F. 1992 Three-dimensional optimal perturbations in viscous shear flow. *Phys. Fluids* A **4**, 1637–1650.

Chang, C.-L. & Malik, M. R. 1994 Oblique-mode breakdown and secondary instability in supersonic boundary layers. *J. Fluid Mech.* **273**, 323–360.

Coughlin, K. 1996 Coherent structures and intermittent turbulence in channel flows. Part 1. Coherent structures. *J. Fluid Mech.* (submitted).

Dauchot, O. & Daviaud, F. 1995*a* Finite amplitude perturbation and spots growth mechanism in plane Couette flow. *Phys. Fluids* **7**, 335–343.

Dauchot, O. & Daviaud, F. 1995*b* Streamwise vortices in plane Couette flow. *Phys. Fluids* **7**, 901–903.

Drazin, P. G. & Reid, W. H. 1981 *Hydrodynamic Stability*. Cambridge University Press.

Dubrulle, B. & Nazarenko, S. 1994 On scaling laws for the transition to turbulence in uniform-shear flows. *Europhys. Lett.* **27**, 129–134.

Ellingsen, T. & Palm, E. 1975 Stability of linear flow. *Phys. Fluids* **18**, 487–488.

Elofsson, P. A. & Alfredsson, P. H. 1995 Experiments on nonlinear interaction between oblique Tollmien–Schlichting waves. In *Laminar-Turbulent Transition* (ed. R. Kobayashi). Springer.

Farrell, B. F. 1988 Optimal excitation of perturbations in viscous shear flow. *Phys. Fluids* **31**, 2093–2102.

Fasel, H. & Thumm, A. 1991 Direct numerical simulation of three-dimensional breakdown in supersonic boundary layer transition. *Bull. Am. Phys. Soc.* **36**, 2701.

Finlay, W. H., Keller, J. B. & Ferziger, J. H. 1988 Instability and transition in curved channel flow. *J. Fluid Mech.* **194**, 417–456.

Fischer, T. M. & Dallmann, U. 1991 Primary and secondary instability analysis of a three-dimensional boundary-layer flow. *Phys. Fluids* A **3**, 2378–2391.

Gathmann, R. J., Si-Ameur, M. & Mathey, F. 1993 Numerical simulations of three-dimensional natural transition in the compressible confined shear layers. *Phys. Fluids* **5**, 2945–2968.

Gustavsson, L. H. 1991 Energy growth of three-dimensional disturbances in plane Poiseuille flow. *J. Fluid Mech.* **224**, 241–260.

Hall, P. & Horseman, N. J. 1991 The linear inviscid secondary instability of longitudinal vortex structures in boundary-layers. *J. Fluid Mech.* **232**, 357–375.

Hamilton, J. M. & Abernathy, F. H. 1994 Streamwise vortices and transition to turbulence. *J. Fluid Mech.* **264**, 185–212.

Hamilton, J. M., Kim, J. & Waleffe, F. 1995 Regeneration mechanisms of near-wall turbulence structures. *J. Fluid Mech.* **287**, 317–348.

Henningson, D. S. 1995 Bypass transition and linear growth mechanisms. In *Advances in Turbulence V* (ed. R. Benzi). Kluwer.

Henningson, D. S., Lundbladh, A. & Johansson, A. V. 1993 A mechanism for bypass transition from localized disturbances in wall bounded shear flows. *J. Fluid Mech.* **250**, 169–207.

Herbert, T. 1988 Secondary instability of boundary layers. *Ann. Rev. Fluid Mech.* **20**, 487–526.

Joslin, R. D., Streett, C. L. & Chang, C. L. 1993 Spatial direct numerical simulations of boundary-layer transition mechanisms: Validation of PSE theory. *Theor. Comput. Fluid Dyn.* **4**, 271–288.

Kawakami, M., Elofsson, P. & Alfredsson, P. H. 1997 Experiments on the stability of streamwise streaks in plane Poiseuille flow. *Tech. Rep.* TRITA-MEK 16. Department of Mechanics, Royal Institute of Technology (KTH), Stockholm, Sweden.

Kim, H. T., Kline, S. J. & Reynolds, W. C. 1971 The production of turbulence near a smooth wall in a turbulent boundary layer. *J. Fluid Mech.* **50**, 133–160.

Kim, J. & Moser, R. D. 1989 On secondary instability in plane Poiseuille flow. *Phys. Fluids* A **1**, 775–777.

Kline, S. J., Reynolds, W. C., Schraub, F. A. & Runstadler, P. 1967 The structure of turbulent boundary layers. *J. Fluid Mech.* **30**, 741–773.

Klingmann, B. G. B. 1992 On transition due to three-dimensional disturbances in plane Poiseuille flow. *J. Fluid Mech.* **240**, 167–195.

Kreiss, G., Lundbladh, A. & Henningson, D. S. 1994 Bounds for threshold amplitudes in subcritical shear flows. *J. Fluid Mech.* **270**, 175–198.

Landahl, M. T. 1975 Wave breakdown and turbulence. *SIAM J. Appl. Maths* **28**, 735–756.

Landahl, M. T. 1980 A note on an algebraic instability of inviscid parallel shear flow. *J. Fluid Mech.* **93**, 243–251.

Le Cunff, C. & Bottaro, A. 1993 Linear-stability of shear profiles and relation to the secondary instability of dean flow. *Phys. Fluids* A **5**, 2161–2171.

Li, F. & Malik, M. R. 1995 Fundamental and subharmonic secondary instabilities of Görtler vortices. *J. Fluid Mech.* **297**, 77–100.

Lundbladh, A., Henningson, D. S. & Johansson, A. V. 1992 An efficient spectral integration method for the solution of the Navier–Stokes equations. *Tech. Rep.* FFA-TN 1992-28. Aeronautical Research Institute of Sweden, Bromma.

Lundbladh, A., Henningson, D. S. & Reddy, S. C. 1994 Threshold amplitudes for transition in channel flows. In *Transition, Turbulence, and Combustion*, Vol. I, (ed. M. Y. Hussaini, T. B. Gatski & T. L. Jackson). Kluwer.

Lundbladh, A. & Johansson, A. V. 1991 Direct simulation of turbulent spots in plane Couette flow. *J. Fluid Mech.* **229**, 499–516.

Matsson, O. J. E. & Alfredsson, P. H. 1992 Experiments on instabilities in curved channel flow. *Phys. Fluids* A **4**, 1666–1676.

Matsubara, M. & Alfredsson, P. H. 1995 Free stream turbulence induced boundary layer transition. *Bull. Am. Phys. Soc.* **40**, 1956.

Mayer, E. W. & Reshotko, E. 1997 Evidence for transient disturbance growth in a 1961 pipe-flow experiment. *Phys. Fluids* A **9**, 242–244.

Morkovin, M. & Reshotko, E. 1990 Dialogue on progress and issues in stability and transition research. In *Laminar-Turbulent Transition* (ed. D. Arnal & R. Michel). Springer.

Orszag, S. A. 1971 Accurate solution of the Orr–Sommerfeld equation. *J. Fluid Mech.* **50**, 689–703.

Orszag, S. A. & Patera, A. T. 1983 Secondary instability of wall-bounded shear flows. *J. Fluid Mech.* **128**, 347–385.

Patel, V. C. & Head, R. 1969 Some observations on skin friction and velocity profiles in fully developed pipe and channel flows. *J. Fluid Mech.* **38**, 181–201.

Reddy, S. C. & Henningson, D. S. 1993 Energy growth in viscous channel flows. *J. Fluid Mech.* **252**, 209–238.

Reshotko, E. 1994 Boundary layer instability, transition and control. *AIAA Paper* 94-0001.

Romanov, V. A. 1973 Stability of plane-parallel Couette flow. Translated in *Funktional Anal. Applics.* **7**, 137–146.

Saric, W. S. 1994 Görtler vortices. *Ann. Rev. Fluid Mech.* **26**, 379–409.

Schmid, P. J. & Henningson, D. S. 1992 A new mechanism for rapid transition involving a pair of oblique waves. *Phys. Fluids* A **4**, 1986–1989.

Schmid, P. J. & Henningson, D. S. 1995 Nonlinear energy density transfer in plane Poiseuille flow. In *Advances in Turbulence V* (ed. R. Benzi). Kluwer.

Schmid, P. J., Reddy, S. C. & Henningson, D. S. 1996 Transition thresholds in boundary layer and channel flows. In *Advances in Turbulence VI* (ed. S. Gavrilakis, L. Machiels & P. A. Monkewitz). Kluwer.

Singer, B. A., Reed, H. L. & Ferziger, J. H. 1989 The effects of streamwise vortices on transition in the plane channel. *Phys. Fluids* A **1**, 1960–1971.

Swearingen, J. D. & Blackwelder, R. G. 1987 The growth and breakdown of streamwise vortices in the presence of a wall. *J. Fluid Mech.* **182**, 255–290.

Tillmark, N. & Alfredsson, P. H. 1992 Experiments on transition in plane channel flow. *J. Fluid Mech.* **235**, 89–102.

Trefethen, L. N., Trefethen, A. E., Reddy, S. C. & Driscoll, T. A. 1993 Hydrodynamic stability without eigenvalues. *Science* **261**, 578–584.

Waleffe, F. 1995*a* Hydrodynamic stability and turbulence: Beyond transients to a self-sustaining process. *Stud. Appl. Maths* **95**, 319–343.

Waleffe, F. 1995*b* Transition in shear flows. Nonlinear normality versus non-normal linearity. *Phys. Fluids* A **7**, 3060–3066.

Waleffe, F. 1997 On a self-sustaining process in shear flows. *Phys. Fluids* A **9**, 883-900.

Yu, X. & Liu, J. T. C. 1994 On the mechanism of sinuous and varicose modes in 3-dimensional viscous secondary instability of nonlinear Görtler rolls. *Phys. Fluids* A **6**, 736-750.

Zikanov, O. Y. 1996 On the instability of pipe Poiseuille flow. *Phys. Fluids* A **8**, 2923–2932.